ABSTRACT

PANDURANGAN, PRADEEP. Defect Identification in GRID-LOCK® Joints. (Under the direction of Dr. Gregory D. Buckner.)

Bonded metallic GRID-LOCK® structures are being adopted for a variety of aerospace applications due to their structural efficiency and damage tolerance. The development of non-destructive evaluation (NDE) methods is necessary to identify bond defects that can lead to failures in these structures. However, this task is complicated by the lack of interior access and complex geometry of GRID-LOCK® components. In this dissertation, the feasibility of various NDE techniques for detecting the existence, location, and extent of bond defects in GRID-LOCK® joints is investigated. Experiments are conducted on customized test structures to compare the effectiveness of optical NDE, ultrasonic C-scans and vibration-based damage detection. Finite element analysis (FEA) is used to interpret experimental results and highlight the advantages of candidate methods. The qualitative effectiveness of optical NDE is further investigated using full-field surface slope measurements (shearography). Because accurate characterization of structural defects is critical to flight safety, a quantitative non-destructive evaluation (QNDE) method using artificial neural networks (ANNs) is developed. This method involves the use of radial basis function networks (RBFNs) trained and validated using FEA simulation data. The effectiveness of this QNDE approach is demonstrated using experimental data from a custom-built optical scanning system.

Defect Identification in GRID-LOCK® Joints

by

Pradeep Pandurangan

A dissertation submitted to the Graduate Faculty of
North Carolina State University
in partial fulfillment of the
requirements for the Degree of
Doctor of Philosophy

Mechanical Engineering

Raleigh, North Carolina
2006

Approved by:

Dr. Kara J. Peters	Dr. Fuh-Gwo Yuan
Dr. Mohammed N. Noori	Dr. Gregory D. Buckner Chair of Advisory Committee

My dad has never failed to inspire me and
my mom has always supported me,
so this one is for them.

Biography

Pradeep Pandurangan was born and brought up in Madras, India. He obtained a Bachelor of Engineering degree from the University of Madras (Sri Venkateswara College of Engineering) in 2002, and a Master of Science degree in Mechanical Engineering from North Carolina State University in 2004. His pursuit of the Doctor of Philosophy in Mechanical Engineering began in 2004 at North Carolina State University. He would like to coach a basketball team some time and he would not be a mechanical engineer if only he was any good at playing the game.

Acknowledgements

I would like to thank,

- My advisor Dr. Gregory D. Buckner. I learned a lot, much more than engineering skills, through my association with him and it was a very rewarding experience.

- The Goodrich Corporation, for funding this research.

- Committee members, Dr. Fuh-Gwo Yuan, Dr. Kara J. Peters and Dr. Mohammad N. Noori, for their valuable suggestions.

- Past and present members of the Electro-Mechanics Research Lab, including Dr. Soheil Saadat, Dr. Heeju Choi, Arun Veeramani , Shaphan Jernigan and Nicholas Jardine, for sharing their expert opinions and for making lab life tolerable.

- Faculty and staff of the Department of Mechanical and Aerospace Engineering, especially Mr. Rufus (Skip) Richardson and Mr. Mike Breedlove for fabricating test specimens.

- Brother-in-law, friends and family, for their support.

Table of Contents

List of Tables

List of Figures

1 Introduction

1.1 Background

In October of 2003, the Goodrich Corporation initiated three sponsored research fellowships at North Carolina State University's Department of Mechanical and Aerospace Engineering: the Goodrich Doctoral, Undergraduate, and Faculty Fellowships. The purpose of these three-year fellowships was to establish research collaboration in the area of structural health monitoring (SHM) with aerospace applications. Subsequently, the Goodrich Aerostructures group proposed a specific topic involving investigation of nondestructive evaluation (NDE) methods for GRID-LOCK® structures. This dissertation summarizes research accomplishments during three years of work done to achieve this objective.

1.2 GRID-LOCK® Structures

GRID-LOCK® technology, recently developed and patented by the Goodrich Corporation, is an innovative method of joining structural components with simple tongue and groove joints (Figure 1.1). The simplest GRID-LOCK® structure consists of two precision-machined metal parts: a base with integral ribs and a cover with integral grooves (Figure 1.2). The ribs of the base mate with the grooves of the cover and the joint is formed by an epoxy. Multi-directional ribs are machined in the base resulting in a cellular type construction. The result is a structurally efficient, double-skinned, ribbed-core structure that is approximately twice as strong and stiff as a stiffened-skin or isogrid structure of equal weight [1].

Salient features of GRID-LOCK® structures include high strength to weight ratios, resistance to corrosion, damage tolerance and flexibility in design to eliminate unwanted vibration modes. In addition, the GRID-LOCK® structural technology facilitates easy machining and assembly leading to reduction in costs.

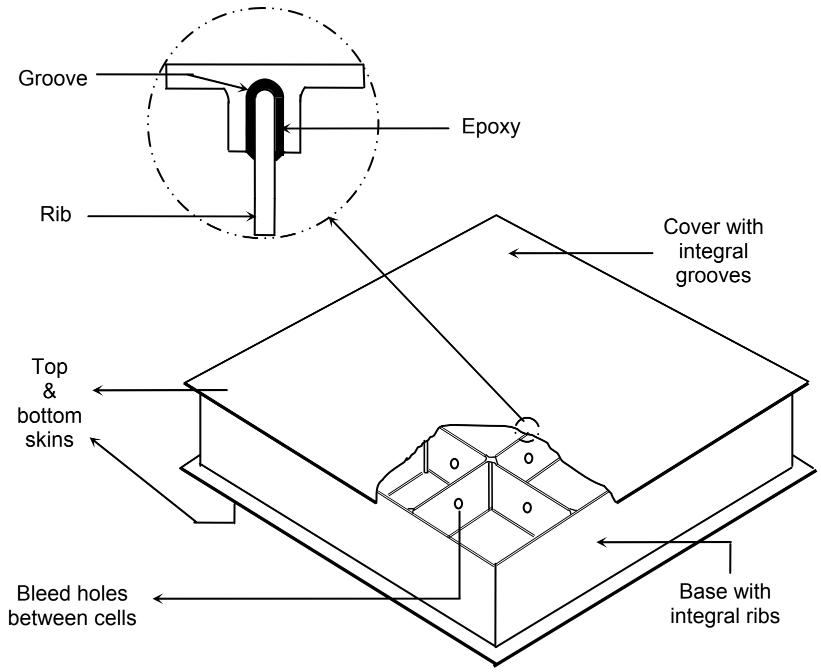

Figure 1.1- GRID-LOCK® technology

Because of the aforementioned advantages, GRID-LOCK® technology has found widespread use in the aerospace industry, including the following:

- AV-8B Harrier bulkheads
- Rigid cargo barriers for Boeing 727, MD-11/MD-10 and A300-600 civil aircraft
- Payload applications for space products, e.g. truss structures for the Hughes HS702 and other mobile satellites
- F-16 fighter aircraft nose, landing gear doors
- C-5 transport aircraft pylons and nacelles systems

Figure 1.2 - GRID-LOCK® control surface

Recently, GRID-LOCK® structures replaced honeycomb structures on the wing tail and fin sections of the F-15 E fighter aircraft (Figure 1.3). Parts of the F-15 E that were replaced include ailerons, wing tips, flap shroud, leading/trailing edges of horizontal stabilators and vertical tail sections. These structures experience extreme loading conditions in harsh operating environments and a limited number of horizontal stabilator base and cover separation failures have been reported [2]. It is known that these failures originate at the epoxy bonded internal joints of these structures. Advanced NDE techniques are needed to inspect the internally bonded joints of GRID-LOCK® structures and prevent such failures. The primary difficulty associated with inspection is that once assembled, accessibility to the interior is severely restricted. Permanent sensor placement for continuous monitoring is not viable considering the harsh operating environments of these structures.

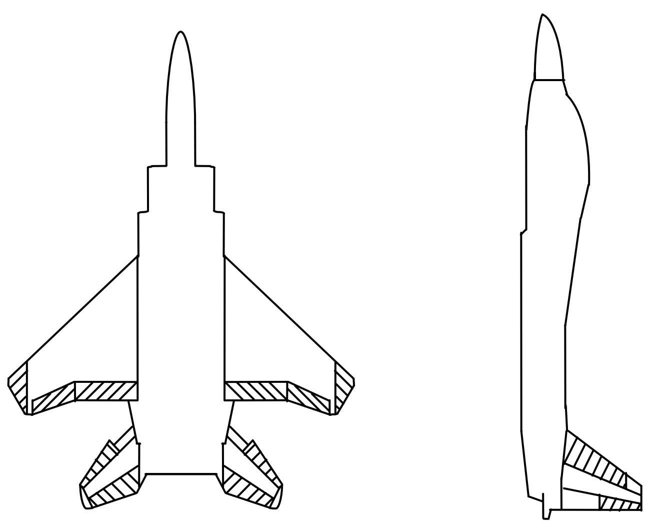

Figure 1.3 - GRID-LOCK® structures on the F15-E fighter aircraft

1.3 Research Objectives

The primary objective of this research is to investigate various non-destructive evaluation techniques (existing and novel) for defect identification in bonded GRID-LOCK® joints and identify an effective and feasible approach. This investigation relies equally on analytical modeling, computational analysis, and experimental validations using customized GRID-LOCK® test structures with realistic failure modes and reasonable access to sensor measurements.

1.4 Context of this work

The research outlined in this dissertation represents the first known investigation of bond defect identification in GRID-LOCK® structures. However, research involving the NDE of similar high strength, low weight aircraft structures (including composite, honeycomb and skin stiffened metallic panels) has been extensive. Although the construction of skin stiffened metallic panels is similar in some respects to GRID-LOCK® technology, their stiffeners are bonded or riveted to the skin while GRID-LOCK® stiffening ribs and grooves are integral to the skin. Previous investigations of damage detection for skin stiffened metallic panels have focused primarily on vibration based techniques including the use of transmissiblities [3], operational deflection shapes [4], modal strain energy [5,6], and frequency response functions [7].

1.5 Organization of Dissertation

This dissertation is a compilation of the three journal papers, each constituting a separate chapter.

The first paper (Chapter 2), entitled '*Vibration analysis for damage detection in metal-to-metal adhesive joints*' [8], describes the use of experimental and computational approaches to investigate service-induced defects in metal-to-metal adhesive joints. Finite element analysis (FEA) is utilized in conjunction with experimental vibration testing to conclude that modes that produce higher stress in defect areas exhibit largest variations in identified modal parameters. The paper also describes the use of a custom pendulum hammer to deliver consistent impacts at precise locations, effectively avoiding non-linearities in structural dynamic response.

The second paper (Chapter 3), entitled '*Assessment of Damage Detection Methods in GRID-LOCK® Structures*' [9], outlines investigations undertaken to detect disbond in GRID-LOCK® joints using three methods (vibration-based damage detection, optical NDE and ultrasonic C-scan). Ultrasonic C-scan proved ineffective in disbond detection due to the complex tongue and groove joint geometry and the lack of access to internal joints. Optical NDE is shown to be superior in defect identification, and FEA reveals that optical NDE has the potential to detect alternate failure mechanisms.

The third paper (Chapter 4), entitled '*Defect Identification in GRID-LOCK® Joints*' [10], describes the use of full-field surface slope measurement (shearography) and a custom built optical scanning system for bond defect identification in GRID-LOCK® structures. Because only qualitative information can be discerned from visual examinations of shearograms, a method for quantitative non-destructive evaluation using a scanning optical probe is developed. This method utilizes the pattern recognition capabilities of radial basis function networks (RBFNs) for bond defect identification and classification.

References

[1] http://www.aerostructures.goodrich.com/html/gridlock.asp,Goodrich Corporation Aerostructures group, 850 Lagoon Drive, Chula Vista, California 91910-2098, USA.

[2] Jason Smith, F-15, Flying Safety magazine - U.S Department of the Air Force, 60 (1-2) (2004) 11-13.

[3] Worden, K., Manson, G., and Allman, D. (2003). Experimental Validation of a Structural Health Monitoring Methodology: Part I. Novelty Detection on a Laboratory Structure. Journal of Sound and Vibration, *259*(2), 323-343.

[4] Jin, S. Frank Pai, P, Locating structural defects using operational deflection shapes, Journal of Intelligent Material Systems and Structures, 11 (8), August, 2000, pp 613-630

[5] Pereyra, Leopoldo R., Osegueda, Roberto A.; Carrasco, Cesar; Ferregut, Carlos, Detection of damage in a stiffened plate from fusion of modal strain energy differences Proceedings of the International Modal Analysis Conference - IMAC, v 2, 2000, p 1556-1562

[6] An experimental appraisal of the strain energy damage location method Worden, K. ,Manson, G.; Allman, D.J, Key Engineering Materials, v 204-205, Damage Assessment of Structures, 2001, p 35-46

[7] Bovio, I., Monaco, E.; Arnese, M.; Lecce, L., Damage detection and health monitoring based on vibration measurements and recognition algorithms in real- scale aeronautical structural components Key Engineering Materials, v 245-346, 2003, p 519-526

[8] Pandurangan P, Buckner GD, ‘Vibration Analysis for Damage Detection in Metal-to-metal Adhesive Joints’, *Experimental Mechanics*, 46 (5), 601-607, Oct 2006.

[9] Pandurangan P, Buckner GD, ‘Assessment of Damage Detection Methods in GRID-LOCK® structures’, *Mechanical Systems and Signal Processing*, Accepted Oct 2006.

[10] Pandurangan P, Buckner GD, ‘Defect Identification in GRID-LOCK® joints’, *NDT & E International*, Submitted Nov 2006.

2 Vibration analysis for damage detection in metal-to-metal adhesive joints

Abstract

Vibration based non-destructive evaluation shows promise for damage detection in metal-to-metal adhesive joints. This research investigates an experimental technique to diagnose damage in single-lap adhesive joints subject to cyclical tensile loading. Vibration analysis reveals that damage can be correlated with changes in identified modal damping ratios. Constant amplitude forcing functions are employed to eliminate amplitude-dependent nonlinearities in the dynamic response profiles. Damping estimates obtained from time-domain analyses correlate well with damage magnitudes. Finite element modal analysis of the lap joints supports the experimental results.

Keywords: metal-to-metal adhesive joints; non-destructive evaluation; vibration analysis; damage detection; modal damping ratio

2.1 Introduction

The use of adhesives in metal-to-metal structural joints offers several advantages, namely higher strength to weight ratios and uniform distribution of stresses [1,2]. However, adhesive joints have found limited applications due to a lack of reliable non-destructive evaluation (NDE) methods [3,4]. NDE of adhesive joints is complicated by the composite nature of their construction involving materials with large differences in material properties. Most NDE techniques for adhesive joints focus on detecting defects like cracks, voids or porosity in the adhesive layer [4,5,6]. These techniques do not provide indications regarding the strength of adhesion, a phenomenon predominant only at the joint interface [7,8,9].

The need for robust NDE techniques that can effectively assess both adhesive and cohesive properties drives research in this field. Sophisticated techniques have been investigated, including, neutron radiography [10], acoustic emission [11], thermography [12], fiber optics [13] x-ray radiography [14] and lamb waves [15]. Despite the documented merits of these approaches, their implementation onto complex structures with limited access to the joints remains suspect.

Vibration analysis (VA) is a well known NDE approach for damage detection in structures [16]. VA uses the dynamic response of a structure to determine its state of health. Damage in a structure can be correlated to changes in its physical parameters, such as mass and stiffness. These changes can be observed as changes in modal parameters (natural frequencies, mode shapes, and modal damping). A principle advantage of “global techniques” like VA is that the approximate location of the fault need not be known in advance, unlike “local techniques” such as eddy current and ultrasonic inspection [17].

Research utilizing VA techniques to identify modal damping (MD) coefficients in adhesive joints has to date yielded mixed results. Shiloh, et al. [18] subjected adhesive joints to artificial aging and found increases in MD with aging. They also reported that increases in MD can be correlated to reductions in shear strength of the joints caused by aging. Vaziri, et al. [19] experimentally investigated the dynamic response of adhesively bonded lap joints with voids of various sizes. They found that MD decreased with increases in void size. Yang, et al. [20] induced strength reductions in double lap composite joints by varying the area of surface preparation before bonding. They reported consistent increases in MD with increases in unprepared surface fraction. Khalil and Kagho [21] introduced voids and disbonds at different locations on adhesive lap joints. Their results showed nonlinear changes in MD with respect to defect location and size. Srivatsan, et al. [22] measured variations in MD of double lap adhesive joints due to improper surface preparation, artificially induced porosity, improper curing, and static loading. In the latter three cases they found no appreciable change in MD.

The absence of conclusive correlations between damage and changes in estimated MD coefficients can be attributed to two factors. First, the defects considered in previous investigations were manufacturing defects, not service induced defects (SID). In the context of this research, SID refers only to defects that arise from load transmission, not defects resulting from corrosion or aging. SID tends to occur in regions of high stress in the form of micro-cracks in the adhesive, whereas manufacturing defects may occur anywhere in the adhesive layer. Second, the effects of excitation amplitude on estimated MD parameters have not been adequately addressed. Since MD exhibits amplitude-dependent nonlinearities, consistent input excitation is needed to identify changes in MD occurring associated with damage. The research presented here correlates changes in modal parameters to SID in metal-to-metal adhesive joints. To account for the effects of amplitude-dependent nonlinearities on modal damping ratios, structural excitation parameters (location, amplitude, duration) are carefully controlled.

2.2 Estimation of damping by vibration analysis

In order to use MD as a damage indicating parameter it must be estimated precisely. There exist several methods to estimate MD [23], though the accuracy of these estimates can vary with the method of measurement [24]. Simpler methods (e.g. the half power points method [25]) are more restrictive in their underlying assumptions and require less computational effort. Conversely, sophisticated methods require additional effort but can reduce variability in MD estimates (e.g. the free-decay envelope method [26]). Up to 250% variations in MD ratios estimated from the frequency domain (half power points) and time domain (free-decay envelop method) have been reported [26].

Researchers investigating VA techniques for adhesive joints have predominantly used the half power points method to estimate MD [19,20,22]. This method is a subjective measurement of MD in the frequency domain based on the sharpness of resonance peaks. This method is prone to bias errors that lead to erroneous estimates of MD, particularly in cases of very low damping [27]. More accurate estimates of MD can be obtained using the free-decay envelope method. This time-domain method involves observing the decay envelope of the dynamic response of the system. MD of a specific mode can be estimated by digitally filtering out the desired resonant frequency from the overall response. The envelope of the filtered signal can be computed with the filtered signal $y(t)$ and Hilbert transform of the filtered signal $\tilde{y}(t)$:

$$E(t) = \sqrt{y^2(t) + \tilde{y}^2(t)} \qquad (1)$$

For linear viscoelastic damping mechanisms this envelope is an exponential profile whose logarithm is a straight line. The slope of this line is a measure of the damping in the mode (Figure 2.1). For small levels of damping, the MD ratio ζ is calculated from the decay envelope:

$$\zeta = \frac{\ln\left[\frac{A_0}{A_n}\right]}{2\pi n} = \frac{m}{2\pi\omega_n} \qquad (2)$$

where ω_n is the resonant frequency of the particular mode, A_0 and A_n are amplitudes of the response at points with *n* peaks between them and *m* is the slope of the logarithm of the decay envelope.

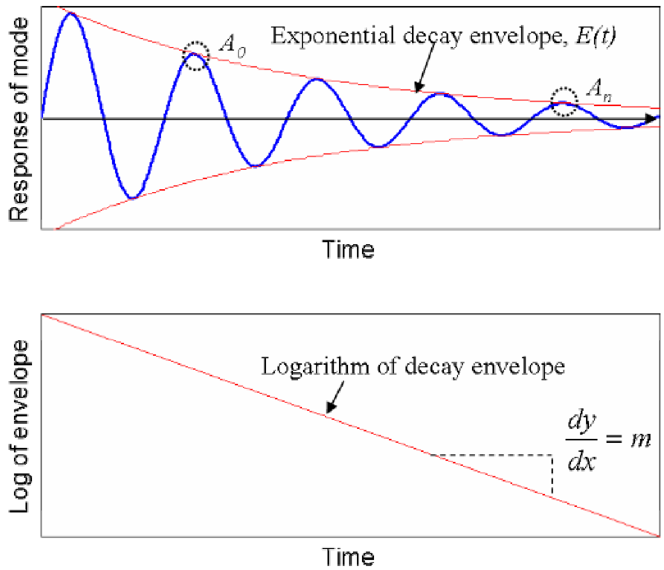

Figure 2.1– Determination of modal damping ratio in the time domain by calculating the rate of decay

The mechanics of damping in structural adhesive joints are inherently nonlinear, and the significance of specific mechanisms is dependent on stress and frequency [28]. For this reason, identified MD values are frequently dependent on the amplitude of excitation. Yang et al. [20] excited double strap adhesively bonded composite joints with small-amplitude impacts (44.5N) and large-amplitude impacts (92.8N). The two impact amplitudes produced 20-35% variations in MD values in undamaged joints. Without consistency in input force amplitudes used for exciting a structure, it might not be possible to differentiate changes in MD estimates associated with damage from those associated with input force amplitude.

2.3 Experiment

Experiments were conducted to investigate the dependence of MD ratios on damage levels in metal-to-metal adhesive joints. Lap joints were fabricated and subjected to a series of tensile loadings and dynamic response measurements.

Tensile loads were applied incrementally to induce various levels of damage in the lap joints. Viscoelastic creep in the adhesive was induced by limiting the loading rate. MD ratios were estimated using the free-decay envelope method based on impact responses of each lap joint. The following sections detail the experimental procedure.

2.3.1 Specimen preparation

Four lap joint samples were prepared in accordance with ASTM D 1002-94 [29], which provides guidelines for tensile testing of metal-to-metal single lap adhesive joints. Samples were fabricated using 6061 aluminum sheet stock (1.6 mm thickness) and Loctite® epoxy 21425. The overlap length of each joint was 19.0 mm, resulting in a total bonded area of 482.6 mm^2. Figure 2.2 shows the geometry of the lap joint specimens. Adherend surfaces were roughened and cleaned with methyl ethyl ketone. Epoxy was then applied to the faying surfaces using spacers (2 mm thick) to ensure a uniform adhesive thickness. Excess adhesive was wiped off and the joints were cured at room temperature (27°C) for a period of 12 hrs.

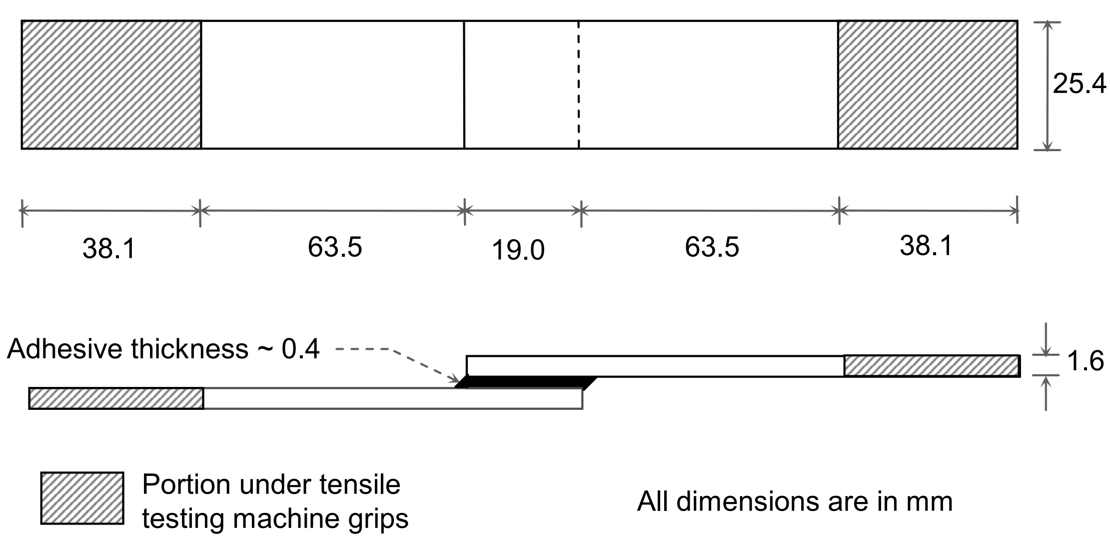

Figure 2.2 – Lap joint geometry

2.3.2 Procedure

The first lap joint specimen was loaded to failure (1960.0 N) in an Instron® 4400R tensile testing machine (Figure 2.3a) to establish a baseline for the remaining tests. The three remaining specimens were subjected to axial loads ranging from 1400.0 N to 1800.0 N in five successive stages. Each stage consisted of three consecutive loads to a given peak value followed by a return to no the load condition (Figure 2.3b). The crosshead speed of the tensile testing machine was maintained at 0.508 mm/min during loading and unloading.

Experimental VA (Figure 2.4) was performed on each specimen before and after each loading stage. The process involved three fundamental phases: (1) excitation of the structure, (2) measurement of the dynamic response and (3) processing of the response to extract modal parameters [30]. The same end of the specimen being tested was clamped using a vice to obtain “fixed–free” boundary conditions. Variations in boundary conditions were minimized by carefully controlling the position of the specimen in the vice (with mechanical stops) and the vice load. The specimen was then struck with an impact hammer and the response was measured using a PCB 353B65 accelerometer and a PCB 482A16 signal conditioning amplifier. Each VA test consisted of four separate dynamic response measurements. The modal parameters were determined for each measurement and the average of the four was noted.

Because it was difficult to generate consistent impact forces using a hand held instrumented impulse hammer, a customized pendulum impact hammer was fabricated (Figure 2.4). This 10.0 g pendulum hammer allowed precise and repeatable control of impact amplitude, angle, location and duration. It also eliminated multiple impacts and provided the excitation consistency needed for accurate estimation of MD ratios. Each impact was delivered at a distance of 12.7 mm from the free end along the axis of the specimen. The accelerometer was located at a distance of 12.7 mm from the clamped end along the axis of the specimen. The effect of location of the accelerometer and impact was studied extensively by conducting roving tests (fixing the accelerometer at different sensing locations and moving the impact location). From the tests it was deduced that the resonant peaks in the response spectrum produced an almost equal intensity if the accelerometer was located in the aforementioned location.

a)

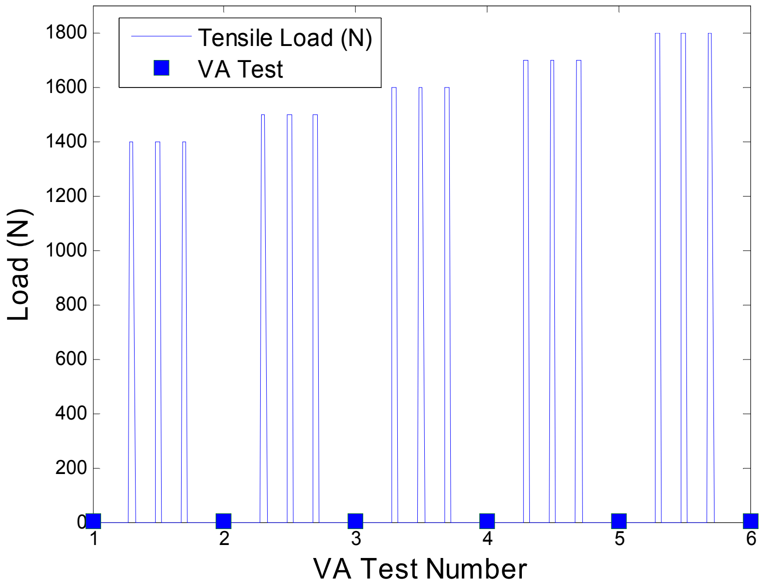

b)

Figure 2.3 – a) Lap joint specimen in the grips of the tensile testing machine, b) Tensile loading and VA testing sequence

Response data was filtered using a Krohn-Hite 3364 low-pass filter with a 2.0 kHz cutoff frequency. Data was acquired using xPC Target™ at a sampling frequency of 6.4 kHz and processed using MATLAB®. Modal parameters of a specific mode were calculated by separating the response of the particular mode from the overall response by designing eighth-order Butterworth band-pass filters in MATLAB®.

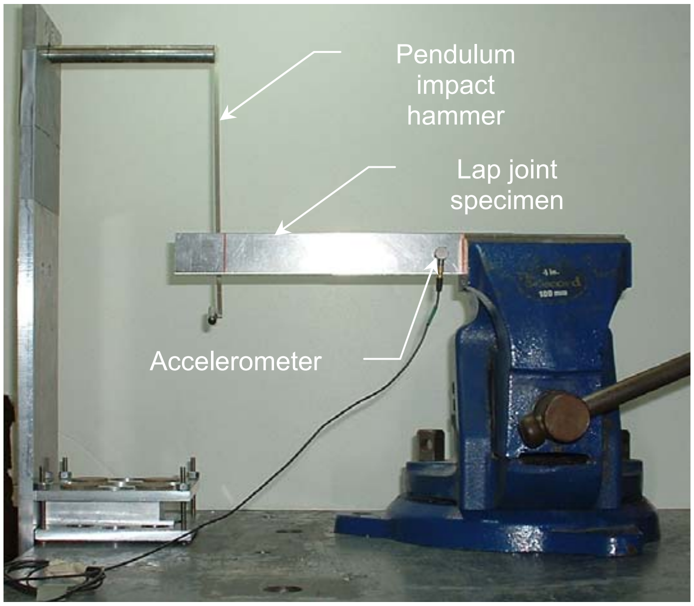

Figure 2.4– Experimental VA setup

2.4 Results

A typical frequency spectrum of the dynamic response for undamaged lap joint specimens is shown in Figure 2.5. Three resonant peaks corresponding to the first three bending modes can be clearly identified.

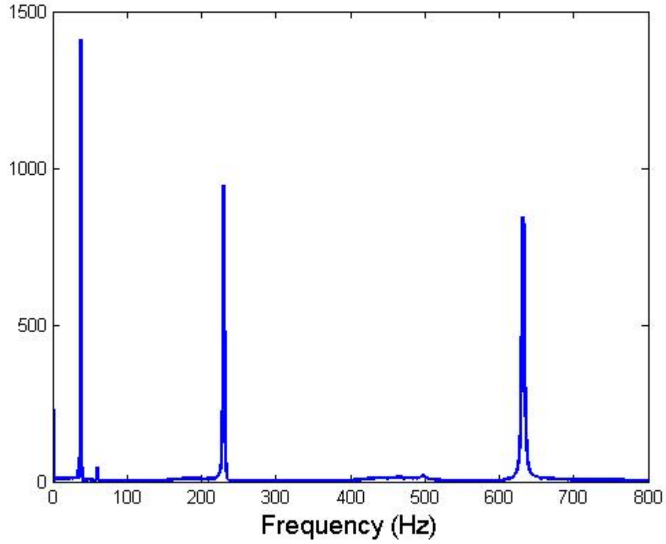

Figure 2.5– Typical frequency spectrum for undamaged specimens

Variations in estimated natural frequencies and MD ratios (normalized by levels corresponding to the undamaged condition) for three specimens subjected to the complete sequence of tensile loading and VA testing are presented in Figures 2.6 and 2.7. Natural frequencies and modal damping ratios of the three modes (averaged across all three specimens while in their healthy state) are also shown.

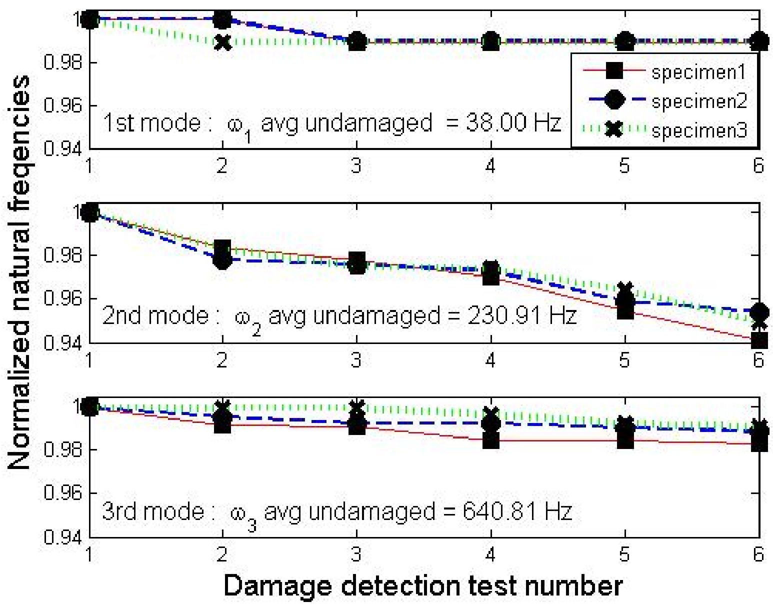

Figure 2.6– Variation in natural frequencies after each stage of loading (values are normalized by natural frequencies of an undamaged specimen)

These plots reveal that natural frequencies tend to reduce and MD ratios tend to increase after each loading stage. Among the three modes for each specimen there is a 40%-250% variation in MD ratios and a 1%-6% variation in the natural frequencies over the course of cyclical loading. The modal parameters of the second mode show the most variation. The second mode shows a 4%-6% decrease in natural frequency and a 150%-250% increase in MD ratio as load levels progress. The results demonstrate that MD ratios are much more sensitive to damage than natural frequencies.

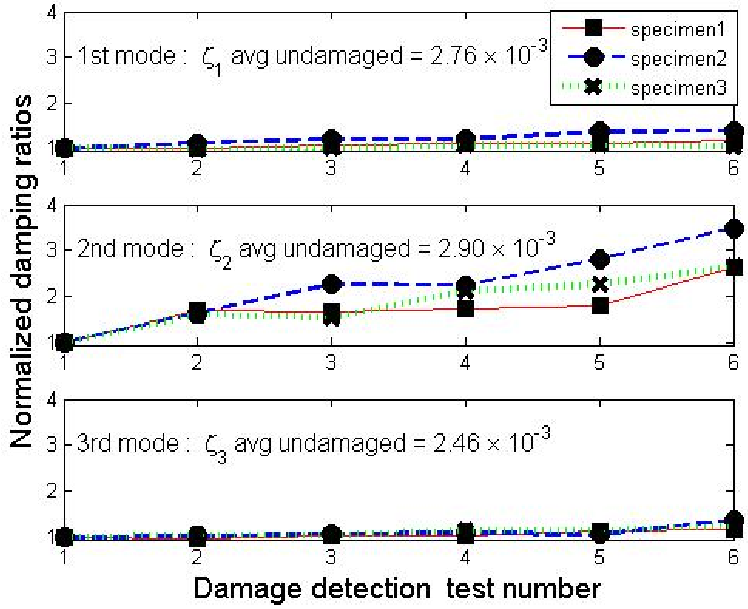

Figure 2.7– Variation in modal damping ratios after each stage of loading

(values are normalized by modal damping ratios for an undamaged specimen)

Load-extension plots for two specimens, one healthy and one that had undergone complete sequence of tensile loading and VA testing, are shown in Figure 2.8. The plot associated with the healthy specimen (Figure 2.8a) reveals no yielding, while the plot associated with cyclical loading (Figure 2.8b) reveals a significant change in slope indicating that yielding has occurred. For the peak tensile loads applied this specimen (1800.0 N), the corresponding stresses in the aluminum adherends (45.0 MPa) is well below their yield strength (250.0 MPa). This indicates that yielding has occurred in the adhesive only, and is caused by the sequential loading and unloading of the joint to high states of stress. The differences in these profiles verify that damage was induced by the chosen loading scheme, and that changes in identified modal parameters (Figures 2.6 and 2.7) were associated with damage in the adhesive.

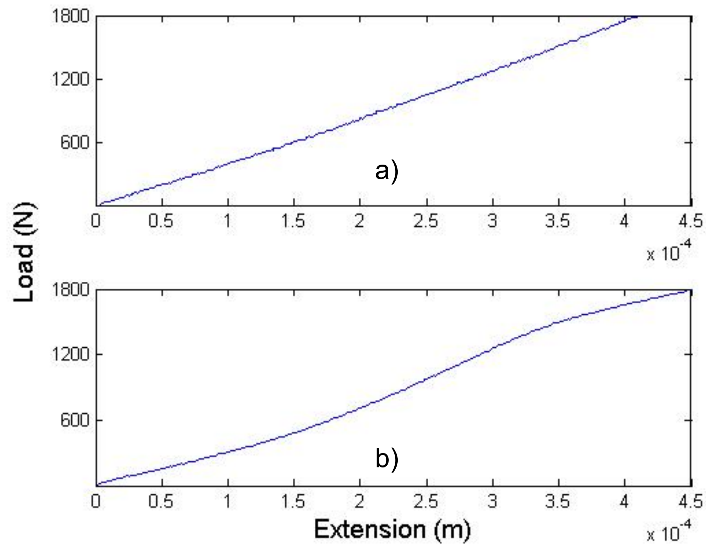

Figure 2.8– Tensile load vs. extension curves a) Healthy specimen,
b) Specimen undergoing full regimen of tensile testing

2.5 Finite element analysis (FEA)

The experimental results indicate that the first and third modes are relatively insensitive to damage when compared to the second mode. In order to gain more insight into this behavior, a 2D finite element model of the lap joints was developed using ANSYS®. A total of 76 four-noded SHELL63 elements were used to model the lap joint. All nodal degrees of freedom at one end were constrained to simulate the fixed-free condition (Figure 2.9). The material properties of the adherend and adhesive for this model are given in Table 2.1.

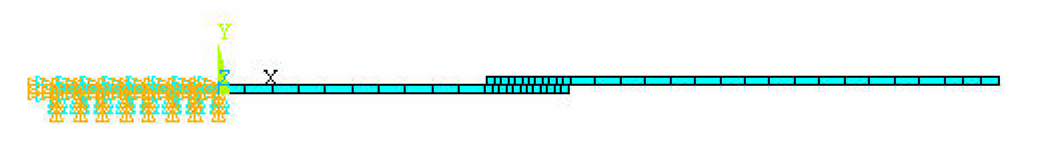

Figure 2.9 – Finite element model of lap joint specimen with constraints

Table 2.1– Material properties used in the FEA specimen model

Material	Young's modulus (GPa)	Poisson's ratio	Density (Kg/m^3)
Adherend, Aluminum	64.0	0.33	2700.0
Adhesive, Epoxy	3.0	0.31	1500.0

A modal analysis of this FEA model yielded the natural frequencies listed in Table 2.2 and the corresponding mode shapes shown in Figure 2.10. Torsional bending modes were excluded as these were not excited during experimental testing. By comparing the FEA natural frequencies to the corresponding experimental natural frequencies (averaged across all three specimens while in their healthy state), it can be deduced that the FEA model is accurate. Overall, the FEA results compare well with the experimental results with a maximum difference of only 2.5% between the two.

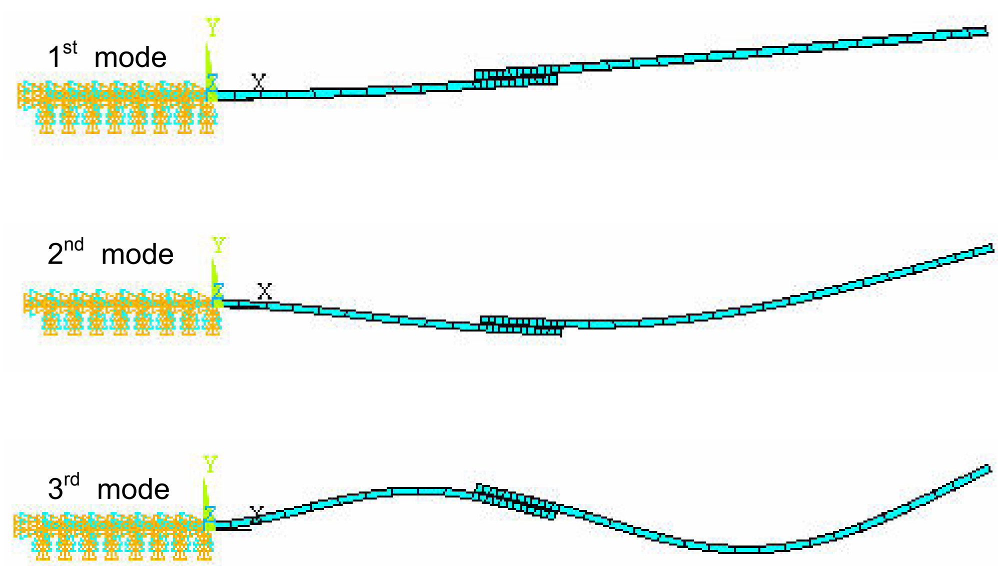

Figure 2.10– Bending mode shapes of lap joint model simulated in ANSYS®

Table 2.2 – Natural frequencies of lap joint specimens: FEA vs. experimental results

	Natural frequencies (Hz)		
	1	2	3
FEA	38.95	229.84	656.47
Experiment	38.00	230.91	640.81

It has been reported that structural damage located in regions of high modal stress significantly affects that particular mode's natural frequency [31]. To investigate the dependence of principal stresses on mode shapes, impact tests were simulated using the validated FEA model. A 100.0 N impact (duration 0.0005 sec) was imparted to the model at each of the experimental locations. The resulting principal stresses in the adhesive layer at each node were extracted. The peak principal stresses associated with each of the three bending modes, averaged among all adhesive layer nodes, are shown in Figure 2.11.

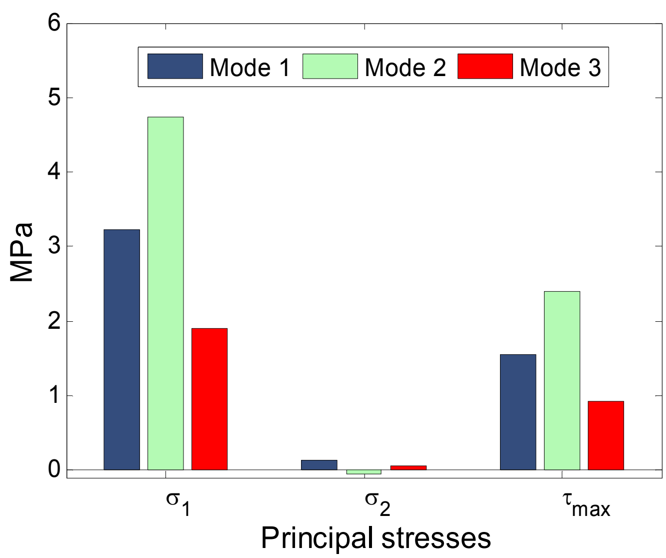

Figure 2.11 - Average of peak principal stresses associated with three bending modes (from nodes along of adhesive layer)

The FEA results of Figure 2.11 indicate that the average of principal stress σ_1 and maximum shear stress τ_{max} among the nodes in the adhesive layer are greatest in the second bending mode. Principal stresses σ_2 due to all the modes are negligible in comparison with the other two stresses. These results reveal that Mode 2 inflicts maximum stress in the damaged adhesive layer. This explains why the modal parameters of the second mode, obtained experimentally (Figures 2.6 and 2.7), show the greatest variation with progressive damage.

2.6 Conclusions

This paper presented experiments conducted to evaluate VA as a tool for damage detection in metal-to-metal adhesive joints. Damage in the joints was induced by a tensile loading scheme (Figure 2.3b), designed to induce adhesive defects similar to those associated with stress-induced creep. The results reveal a significant correlation between damage and MD estimates (40%-250% variation in MD ratios and a 1%-6% variation in the natural frequencies among the three modes for each specimen), indicating that VA may be an effective tool for NDE in structural adhesive joints. Finite element modal analysis of the lap joints agreed well with experimental results (maximum difference of only 2.5% between natural frequencies of experiment and FEA), and provided an explanation for differences in sensitivity to damage for various modes. The mode which inflicts maximum stress to the damaged overlap area (Mode two) has parameters that are most sensitive to damage. Because only marginal changes in natural frequency (1%-6%) were detected with progressive damage, it does not appear to be an effective parameter for damage detection. Future work will investigate similar relationships in bonded larger metallic components with complex geometries to confirm the effectiveness of the methods outlined in this research.

Acknowledgements

The authors would like to thank the Goodrich Corporation for funding this research.

References

[1] Messler, R.W., Joining of Advanced Materials, Butterworth-Heinmann, Boston (1993).

[2] Adams, R.D., Comyn, J., and Wake, W.C., Structural Adhesive Joints in Engineering (Second edition), Chapman & Hall, London (1997).

[3] Schindel, D.W., "Air-coupled Ultrasonic Measurements of Adhesively Bonded Multi-layer Structures," Ultrasonics, 37(3), 185-200 (1999).

[4] Heslehurst, R.B., "Observations in the Structural Response of Adhesive Bondline Defects," International Journal of Adhesion and Adhesives, 19(2-3), 133-154 (1999).

[5] Adams, R.D. and Drinkwater, B.W., "Nondestructive Testing of Adhesively-bonded Joints ," NDT&E International, 30(2), 93-98 (1997).

[6] Nieminen, A.O.K., and Koenig, J.L., "Macroscopic and Modern Microscopic NDE Methods for Adhesive-bonded Structures," International Journal of Adhesives and Adhesion, 1(1), 5-10 (1991).

[7] Bockenheimera, C., Fataa, D., Possarta, W., Rothenfusserb, M., Netzelmannc, D., and Schaeferd, H., "The Method of Non-linear Ultrasound as a Tool for the Non-destructive Inspection of Structural Epoxy-metal Bonds," International Journal of Adhesion and Adhesives, 22(3), 227–233 (2002).

[8] Brotherhood, C.J., Drinkwater, B.W., and Dixon, S., "The Detectability of Kissing Bonds in Adhesive Joints Using Ultrasonic Techniques," Ultrasonics, 41(7), 521–529 (2003).

[9] Segal, E., and Kenig, S., "Acceptance Criteria for Nondestructive Evaluation of Adhesively Bonded Structures," Materials Evaluation, 47(8), 921-927 (1989).

[10] Michaloudaki, M., Lehmann, E., and Kosteas, D., "Neutron Imaging as a Tool for the Non-destructive Evaluation of Adhesive Joints in Aluminum," International Journal of Adhesion and Adhesives, 25(3), 257-267, (2005).

[11] Magalhaes, A.G., and De Moura, M.F.S.F., "Application of Acoustic Emission to Study Creep Behaviour of Composite Bonded Lap Shear Joints," NDT and E International, 38(1), 45-52 (2005).

[12] Meola, C., Bruzzone, A., Giorleo, L., Morace, R.E., and Vitiello, A., “Application of Lock-in Thermography in Non-destructive Evaluation of Adhesively-bonded Aluminum Joints,” Journal of Adhesion Science and Technology, 18(6), 635-654 (2004).

[13] Schulz, W.L., Udd, E., Morrell, M., Seim, J., Perez, I., and Trego, A., “Health Monitoring of an Adhesive Joint Using a Multi-axis Fiber Grating Strain Sensor System,” Proceedings of SPIE - The International Society for Optical Engineering, 3586, 41-52 (1999).

[14] Ashcroft, I.A., Erpolat, S., and Tyrer, J., “Damage Assessment in Bonded Composite Joints,” Key Engineering Materials, 245-346, 501-508 (2003).

[15] Mustafa, V., Chahbaz, A., Hay, D.R., and Brassard, M., “Implementation of Guided Waves for Adhesively Bonded Structures,” Canadian Aeronautics and Space Journal, 43(1), 39-43, (1997)

[16] Doebling, S.W., Farrar, C.R., and Prime, M.B., “Summary Review of Vibration Based Damage Identification Methods,” Shock and Vibration Digest, 30(2), 91-105 (1998).

[17] Vanlanduit, S., Parloo, E., and Guillaume, P., “Combined Damage Detection Techniques,” Journal of Sound and Vibration, 266(4), 815-831 (2003).

[18] Shiloh, K., Eliahu, A., Rosenberg, A., Zilber, R., Buchman, A., and Ungarish, M., “Aging Characterization of Adhesives and Bonded Joints by Non-destructive Damping Measurements,” Journal of Intelligent Material Systems and Structures, 10(5), 353-362 (2000).

[19] Vaziri, A., Nayeb-Hashemi, H., and Hamidzadeh, H. R., “Experimental and Analytical Investigations of the Dynamic Response of Adhesively Bonded Single Lap Joints,” Transactions of the ASME – Journal of Vibration and Acoustics, 126, 84-91(2004).

[20] Yang, S., Gu, L., and Gibson, R.F., “Nondestructive Detection of Weak Joints in Adhesively Bonded Composite Structures,” Composite Structures, 51(1), 63-71 (2001).

[21] Khalil, A.A., and Kagho, A.N., “Non-destructive Testing of Adhesively Bonded Joints Using Vibrational Analysis,” International Journal of Adhesives and Adhesion, 1(2), 121-127 (1991).

[22] Srivatsan, T.S., Mantena, R., Gibson, R.F., Place, T.A, and Sudarshan, T.S., "Electromagnetic Measurement of Damping Capacity to Detect Damage in Adhesively Bonded Material," Materials Evaluation, 47(5), 564-570, (1999).

[23] Hadjian, A. H., Masri, S. F., and Saud, A. F., "A Review of Methods of Equivalent Damping Estimation from Experimental Data," Journal of Pressure Vessel Technology - Transactions of the ASME, 109(2), 236-243 (1987).

[24] Willams, C., and Salawu, O.S., "Damping as a Damage Indication Parameter," Proceedings of the 1997 15th International Modal Analysis Conference (IMAC) -Part 2, Orlando, USA, Feb (1997).

[25] Macioce, P., "Viscoelastic Damping 101," S V Sound and Vibration, 37(4), 8-10 (2003).

[26] Hartwigsen, C.J., Song, Y., McFarland, D.M., Bergman, L.A., and Vakakis, A.F., "Experimental Study of Non-linear Effects in a Typical Shear Lap Joint Configuration," Journal of Sound and Vibration, 277(1-2), 327–351 (2004).

[27] Littler, J.D., "Assessment of some of the Different Methods for Estimating Damping from Full-scale Testing," Journal of Wind Engineering and Industrial Aerodynamics, 57(2-3), 179-189, (1995).

[28] Beards, C. F., Structural Vibration Analysis and Damping, Halsted Press, London (1996).

[29] ASTM D 1002-94, "Test Method for Apparent Shear Strength of Single-lap-joint Adhesively Bonded Metal Specimens by Tension Loading," Annual Book of ASTM Standards, 15.06, ASTM International, 45–48 (1999).

[30] Ewins, D.J., Modal Testing Theory Practice and Application (Second edition), Research Studies Press, Baldock (2000).

[31] Hearn G, Testa R.B., "Modal Analysis for Damage Detection in Structures", Journal of Structural Engineering-ASCE, 117(10), 3042-3063, Oct (1991).

3 Assessment of Damage Detection Methods in GRID-LOCK® Structures

Abstract

Bonded metallic GRID-LOCK® structures are being adopted for a variety of aerospace applications due to their structural efficiency and damage tolerance. However, effective damage detection in these structures is complicated by a lack of interior access. In this paper, the feasibility of various non-destructive evaluation (NDE) techniques for detecting the presence, location, and magnitude of damage in GRID-LOCK® is investigated. Experiments conducted on a GRID-LOCK® test structure reveal that vibration-based damage detection and optical NDE methods are superior to ultrasonic C-scans in detecting disbond defects. Finite element analysis (FEA) is used to interpret experimental results and highlight the advantages of alternate NDE approaches.

Keywords: GRID-LOCK® structures; non-destructive evaluation; ultrasonic inspection; vibration-based damage detection; optical NDE; finite-element analysis

3.1 Introduction

Damage detection in aircraft structures is usually conducted using non-destructive evaluation (NDE) techniques like visual inspection, ultrasonic inspection, eddy current inspection and X-ray radiography [1]. These techniques are well established and have distinct advantages and limitations [2]. Recent technological improvements have enhanced the applicability of these techniques to aircraft structures; specific examples include ultrasonic inspection of bond degradation [3], surface defects inspection using eddy currents [4] and sub-surface defect inspection using X-rays [5]. For sophisticated aircraft structures, however, the effectiveness of these approaches is extremely limited. Modern lightweight construction methods are proving difficult to inspect using these techniques, requiring the development of advanced methods [6].

One such aircraft structure is the GRID-LOCK® technology recently developed by the Goodrich Corporation. GRID-LOCK® is an innovative method of joining structural components with simple tongue and groove joints (Figure 3.1). The simplest GRID-LOCK® structure consists of two precision-machined metal parts: a base with integral ribs and a cover with integral grooves. The ribs of the base mate with the grooves of the cover and the joint is formed by an epoxy. Multi-directional ribs are machined in the base resulting in a cellular type construction. The result is a structurally efficient, double-skinned, ribbed-core structure that is approximately twice as strong and stiff as a stiffened-skin or isogrid structure of equal weight [7].

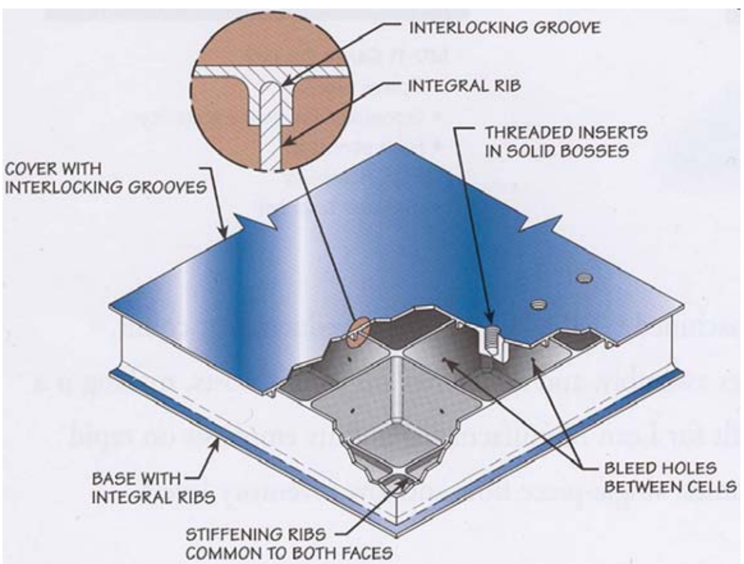

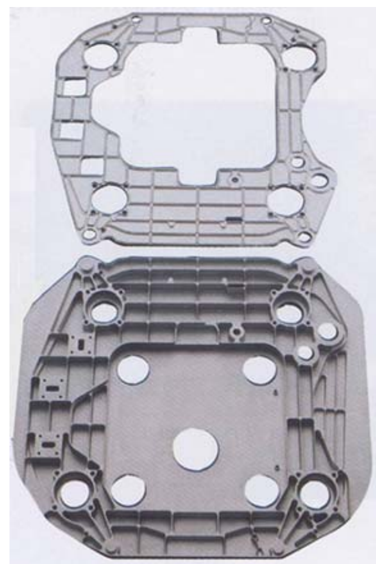

a) b)

Figure 3.1- GRID-LOCK® structures: a) Basic construction,
b) Components of an AV-8B Harrier bulkhead [7]

GRID-LOCK® structures are ideally suited to a variety of commercial, military and space applications. Recently, they replaced honeycomb structures located on the horizontal stabilator of the F-15E fighter aircraft [8]. These structures experience extreme loading conditions in harsh operating environments, and a limited number of base and cover separation failures have been reported [9]. Advanced NDE techniques are needed to inspect the internally bonded joints of GRID-LOCK®

structures and prevent such failures. The primary difficulty associated with inspection is that once assembled, accessibility to the interior is severely restricted. Permanent sensor placement for continuous monitoring is not viable considering the harsh operating environments of these structures.

In this experimental study, the feasibility and effectiveness of ultrasonic inspection, vibration-based damage detection, and optical NDE for detecting defects in GRID-LOCK® joints are investigated. The damage mechanism considered is disbond: an adhesive joint defect characterized by the separation of adhesive and adherend that creates two traction-free surfaces [10]. Disbond leads to the development of stress concentrations and transverse-tearing loads (peel) in the adhesive which are detrimental to joint integrity [11]. Such defects could be service-induced or may also occur during manufacturing; either way their presence in GRID-LOCK® structures is undesirable and needs to be detected. Disbond is induced by internal pressurization of a test structure and the effectiveness of each approach in disbond detection is compared. Finite element analysis (FEA) is used to interpret experimental results and highlight the advantages of alternate NDE approaches.

3.2 Background

Of the three NDE methods investigated in this study, widespread utilization in aircraft structures is currently restricted to ultrasonic inspection. Ultrasonic C-scan utilizes high frequency sound waves to identify defects in solid materials; it is now the industry standard for inspection of aerospace structures such as honeycomb panels [12] and composites plates [13]. Ultrasonic C-scan is preferred because it provides a plan view of test specimen features by depicting them in different colors that represent intensity of measured parameters (amplitude or time-of-flight of ultrasonic waves).

The second technique investigated is vibration-based damage detection [14, 15], an NDE technique that correlates changes in structural dynamic responses to damage within the structure. Despite extensive research on the application of this technique to aircraft structures [16, 17], it has not been widely adopted for this purpose. In fact, the only practical application of this technique has been in the inspection of helicopter transmission systems [18]. However, this method offers a distinct advantage for GRID-LOCK® inspection: it is a global technique that does not need access to interior portions of the structure. Vibration-based damage detection can be implemented using data from time, frequency, or modal domains. Modal data is preferred by most researchers because it is generally easier to interpret and correlate to damage. Among the common modal parameters (natural frequencies, mode shapes, and modal damping ratios), natural frequencies can be estimated with the fewest sensors (most cases require only one optimally located sensor) and can be directly related to stiffness changes.

The third method investigated in this study is an optical NDE method [19] involving the measurement of surface displacements resulting from applied loads. Optical NDE methods use holographic techniques [20, 21] to monitor out-of-plane deformations of a loaded surface; underlying structural defects can be correlated to changes in these measurements. Researchers have employed various methods for loading the test specimen; both mechanical (bending, impact, pressurization, etc.) and thermal loading schemes have been utilized. Internal pressurization is an ideal loading mechanism for GRID-LOCK® structures because of their sealed cellular construction with interconnecting bleed holes. Internal pressurization leads to a uniform load distribution and has been utilized for optical NDE of composite cylinders [22].

3.3 Methods and Materials

This experimental study required the design and fabrication of a GRID-LOCK® test structure. Design specifications were formulated to ensure ease of manufacturability, testing and interpretation of experimental results. Specific requirements of the test structure included:

- Incorporation of realistic GRID-LOCK® features (epoxy-bonded tongue and groove joints, cellular construction, etc.)

- Widely spaced vibration modes to enhance the interpretation of vibration-based damage detection results

- Access to the internally bonded joints for endoscopic inspection

- Secure fixturing to enhance accuracy of response measurements

A test structure satisfying these specifications was designed and fabricated for experimental testing (Figures 3.2, 3.3). The base of this test structure features a lip for securing the specimen during pressurization and testing, effectively constraining all degrees of freedom along its periphery. A Schrader valve was fitted to the largest of four cells in the base for internal pressurization and small bleed holes in the ribs facilitated the distribution of air to each cell. Two sealable inspection ports were incorporated to allow internal inspection of internal bonded joints using an endoscope. This test specimen was machined out of 6061 aluminum using a Haas VF-1 CNC milling machine.

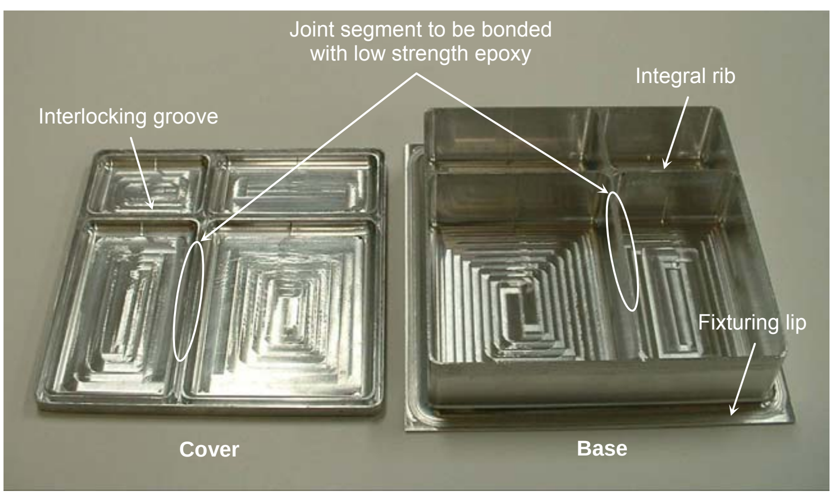

Figure 3.2 – GRID-LOCK® test structure after machining

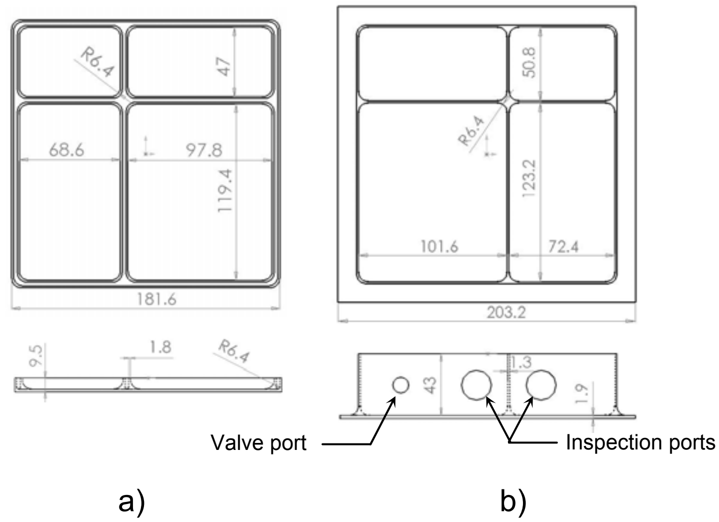

Figure 3.3 - Dimensions of GRID-LOCK® test structure:
a) cover, b) base (dimensions in mm)

Before bonding, the faying surfaces were abraded and cleaned with Methyl Ethyl Ketone (MEK). Two different epoxies, 3M® DP- 460 and Loctite® 21425 were used to bond the base and cover together. The shear strength (ASTM D 1002) of the former is 23400 kPa while that of the latter is 13800 kPa [23]. The epoxy with lower shear strength was used to bond a 50 mm segment of the joint bordering the two largest cells (Figure 3.2). This joint segment bears the maximum loads because it borders the largest cells; finite element analysis revealed that Von Mises stresses in the adhesive layer of this joint segment were significantly (up to eight times) higher than stresses elsewhere in the joint. The epoxy with higher shear strength was used for all remaining joint segments. Both adhesives were cured at room temperature (24°C) for a period of 5 days.

The fixturing lip on the bonded test structure was secured using a steel frame (Figures 3.4 and 3.5) that was bolted to a steel table for experimental pressurization and measurement. This effectively constrained all boundary conditions along the test specimen's perimeter and provided a setup that minimizes the influence of boundary conditions on response measurements.

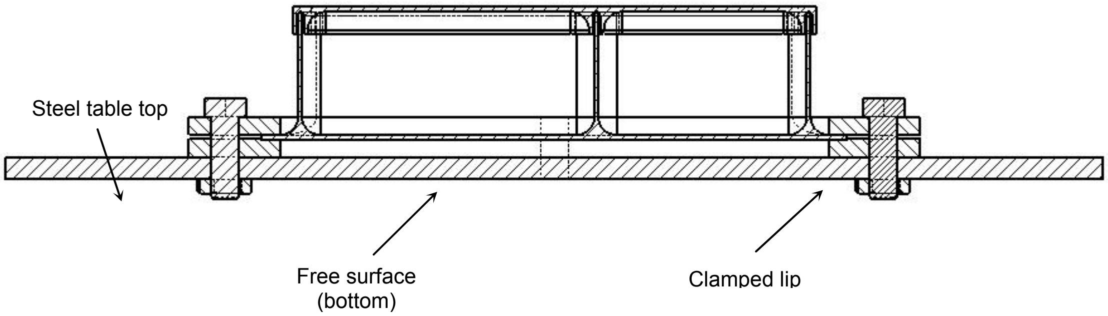

Figure3. 4 - Boundary conditions during pressurization and response measurement

3.3.1 Test Procedures

An ultrasonic C-scan of the bonded test structure was performed prior to internal pressurization for comparison to scans generated after disbond. The test structure was submerged in an ultrasonic immersion tank and scanned using a 10 MHz probe. The test structure was then fixtured and excited using a modal impact hammer (PCB 086C03) and its structural response was measured using a piezoelectric accelerometer (PCB 353B65). The impact and response measurement locations (Figure 3.5) were chosen so that the first three vibration modes were present in the response spectrum with comparable intensity. The response data was acquired at a sampling frequency of 20 kHz using a multi-function data acquisition card (National Instruments PCI-6024E) and LabVIEW™ software.

Table 3.1 – Internal pressurization schedule

Loading stage	Pressure (kPa)	Number of cycles
1	69	20
2	69	20
3	138	20
4	138	20
5	207	20
6	207	20
7	276	20

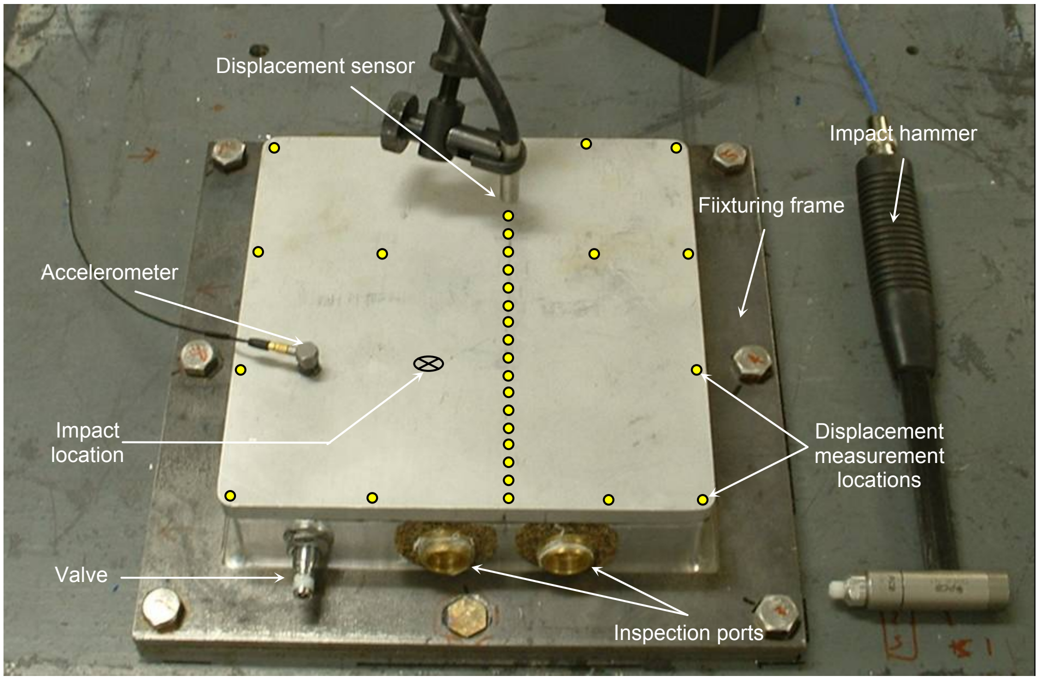

Figure 3.5 - Experimental set up

The test structure was then loaded by regulating its internal pressure in stages (Table 3.1). Each stage consisted of 20 pressurization cycles to a fixed value (69-276 kPa) followed by a return to atmospheric pressure. Displacements of the top surface (cover side) during pressurization were made using a non-contacting fiber optic displacement sensor (Philtec RC-89) with a resolution of 142.0 nm. This displacement sensor was mounted above the test structure using an articulated holder with a magnetic base. Vertical displacements were measured at 32 points along the joints, with a higher spatial resolution (1 measurement per cm) along the weakened joint segment.

After each loading stage, dynamic response measurements were acquired and the inspection ports were opened for visual inspection of the internal bonded joints using an endoscope. After disbond was identified using the endoscope (Figure 3.6), a final set of dynamic response and optical displacement measurements were taken and another ultrasonic C-scan of the structure was performed (Figure 3.7).

3.4 Results

Cyclical internal pressurization of the structure led to disbond along the weakened joint segment (that portion bonded with epoxy of lower shear strength as shown in Figure 3.2) during the seventh loading stage (Table 3.1). Visual inspection of the test structure's interior using an endoscope revealed that disbond occurred along the entire weakened joint segment (Figure 3.6). The endoscopic images confirmed that any variations observed using the three candidate methods were due to disbond and not any other factor. The disbond occurred suddenly, as previous endoscopic inspections (done at the end of each loading stage) did not reveal the existence or propagation of any defect. It is worth noting that there was no external indication of damage to the test structure.

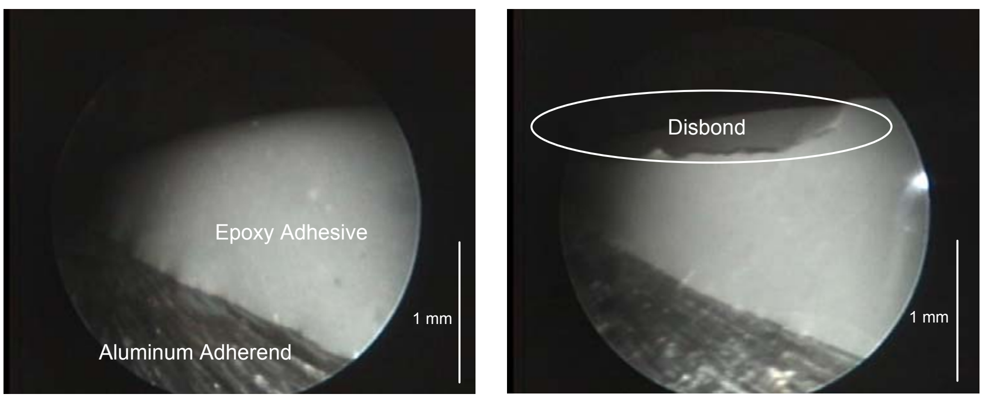

a) b)

Figure 3.6 – Endoscopic imaging of weakened joint segment a) before disbond (after Loading Stage 6), b) after disbond (after Loading Stage 7)

3.4.1 Ultrasonic Inspection

Figure 3.7 compares the ultrasonic C-scans conducted before and after the occurrence of the disbond in the GRID-LOCK® test specimen. Color variations in each scan correspond to variations in energy measured by the probe (signal amplitude). Thinner portions of the test structure reflect more of the ultrasonic energy back to the scanning probe and appear lighter, clearly revealing the internal cellular construction. On the contrary, thicker regions tend to transmit ultrasonic waves and appear darker. Therefore, it is reasonable to expect that joint disbond could be discerned as lighter shades in the C-scans. However, a detailed examination and comparison of the two images in Figure 3.7 does not provide any clear indication of the disbond present at the weakened joint segment.

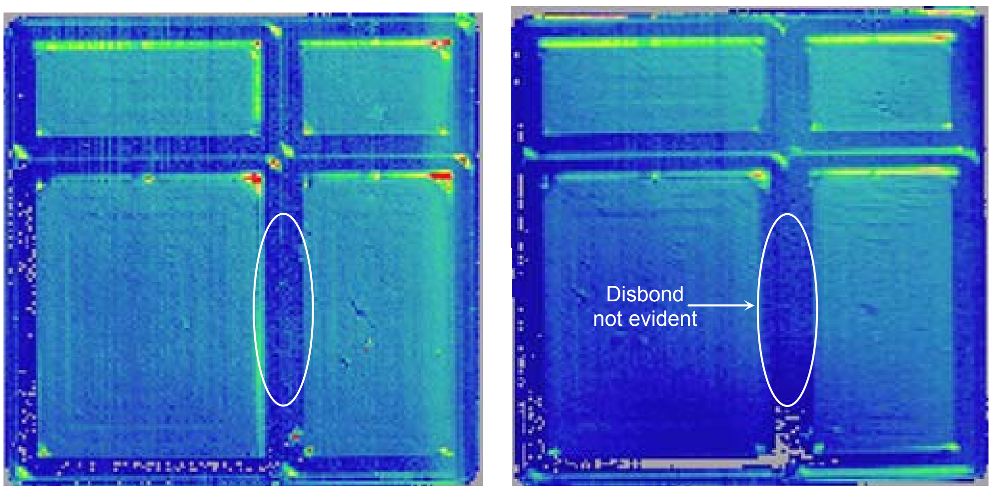

a) b)

Figure 3.7 – Ultrasonic C-scans of the test structure: a) before disbond (prior to Loading Stage 1), b) after disbond (after Loading Stage 7)

3.4.2 Vibration-Based Damage Detection

The first three vibration modes of the test structure were clearly identified from magnitude spectra of the measured accelerometer responses. Comparisons of these spectra before and after disbond showed distinct changes (Figure 3.8); shifts in the three fundamental natural frequencies associated with disbond are presented in Table 3.2. Figure 3.9 shows changes in these natural frequencies as a function of loading stage. This figure reveals significant changes only after the seventh loading stage. These abrupt changes can clearly be related to the sudden occurrence of disbond.

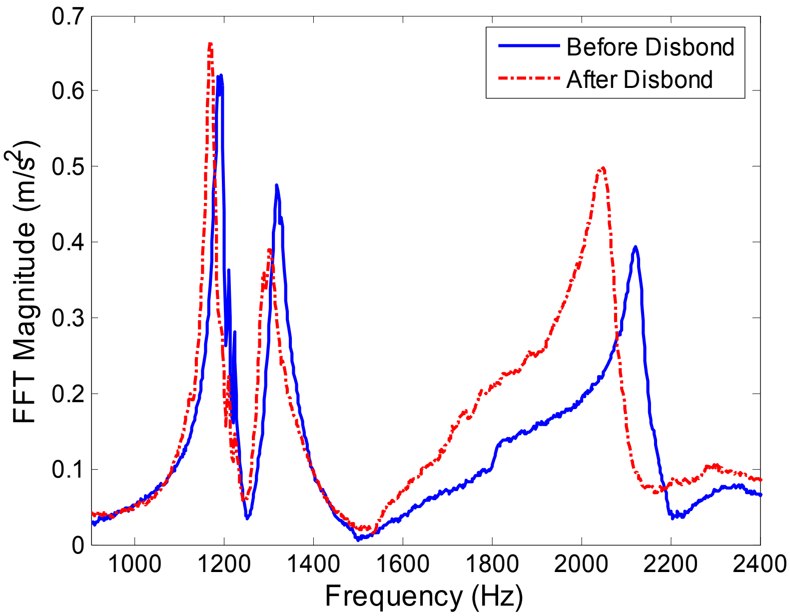

Figure 3.8 – Experimental response spectra before and after disbond

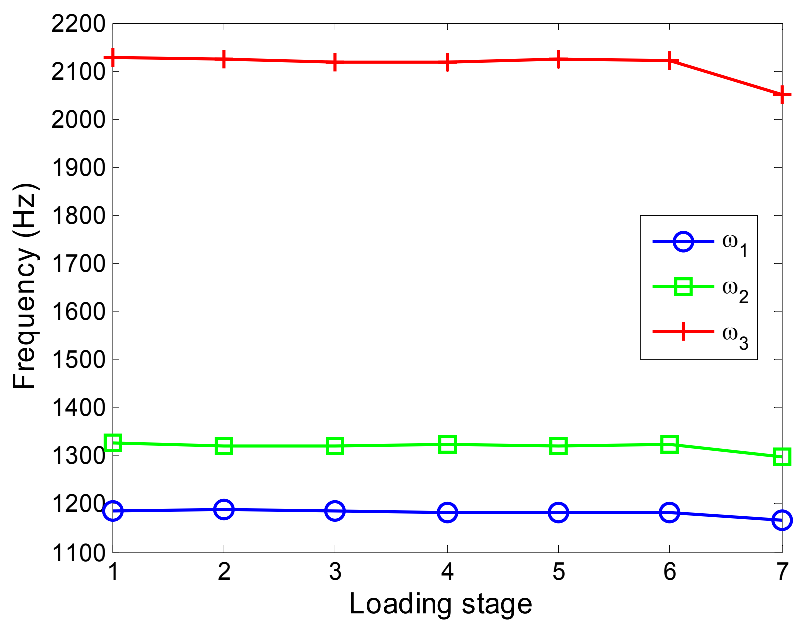

Figure 3.9 - Variation in natural frequencies with loading stages during experiment

Table 3.2– Experimental natural frequencies before and after disbond

Mode	Natural Frequency (Hz)		Change (%)
	Before disbond	After disbond	
1	1186.2	1167.0	-1.6
2	1326.4	1299.2	-2.0
3	2127.9	2049.5	-3.6

3.4.3 Optical Displacement Measurements

Out-of-plane deformations of the top surface (cover side) during pressurization were made using a non-contacting fiber optic displacement sensor. Figure 3.10 compares displacement measurements for an internal pressure of 138 kPa before and after disbond. Note that these measurements are comparable except along the joint segment where disbond has occurred. Along this segment, measurements taken post-disbond were as much as four times greater than those taken before.

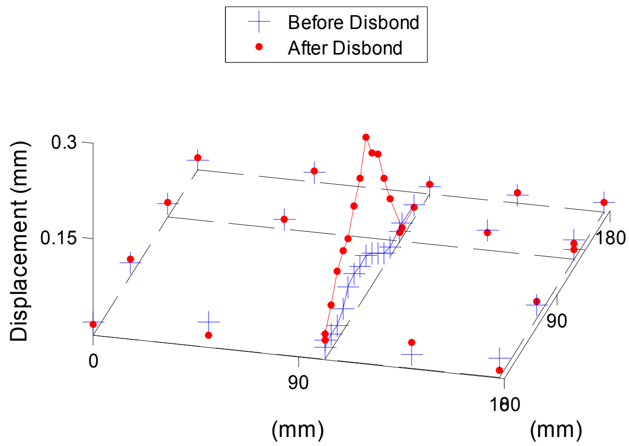

Figure 3.10 – Optical displacement measurements of test structure surface: 138 kPa internal pressure

3.5 Discussion of Experimental Results

The ultrasonic C-scans did not reveal the presence of disbond because the tongue and groove joint geometry cannot be effectively examined using ultrasonic inspection. One of the disadvantages of ultrasonic inspection is that the technique does not always detect planar defects that are perpendicular to the wave front. Complete inspection of these joints (and possible detection of the disbond damage) could be accomplished only if the probe could be oriented parallel to the bondline as shown in Figure 3.11b. However, due to a lack of interior access, the probe can only be positioned vertically as shown in Figure 3.11a. Hence any disbond along the depth of the joint may not be detected using this technique. These drawbacks associated with ultrasonic inspection are highlighted by the experimental results and indicate that it cannot be reliably used for inspection of GRID-LOCK® structures.

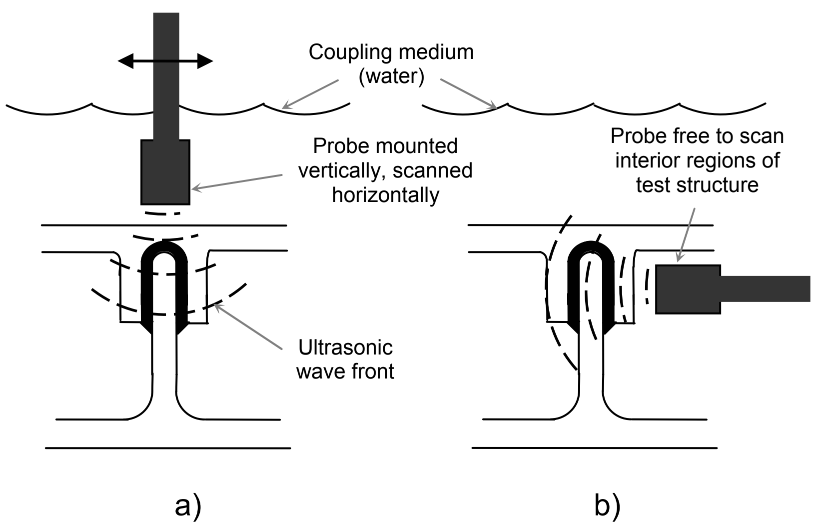

Figure 3.11 - Ultrasonic inspection of test structure:
a) probe mounted vertically, scanning external surfaces,
b) ideally, probe could access interior regions at any orientation

Vibration-based damage detection and optical displacement measurements successfully indicated disbond in the test structure, information would be useful for assessing the severity of damage and characterizing the integrity of the structure. The former technique, however, did not provide information regarding the location or extent of the disbond. Additionally, the dynamic response measurements (Figs. 8, 9, and Table 3.2) could prove to be sensitive to variations in test conditions (boundary and environmental) that were eliminated during the experiment. Extracting disbond size and location information from natural frequency measurements requires the solution to an inverse problem [24]. These problems usually do not have unique solutions (except for structures with simple geometries like beams and plates) because different combinations of defect types, locations, and sizes can produce identical changes in natural frequencies. Another viable method of determining disbond size and location involves mode shape measurement [25], which requires averages of multiple noise-free response measurements at many locations leading to tedious data processing. On the other hand, displacement measurements (Figure 3.10) give a clear indication of disbond location and a rough estimate of its size with just a few, easy to acquire measurements.

3.5.1 Finite Element Analysis

Because vibration-based damage detection and optical displacement measurements successfully indicated disbond in the test structure, FEA was used to investigate the extended capabilities of these techniques. For this study, a finite element model of the test structure was developed in ANSYS® using a total of 57,950 ten-node SOLID92 elements (Figure 3.12). All degrees of freedom for nodes along the lips were constrained to simulate experimental boundary conditions. The material properties used in the model are given in Table 3.3.

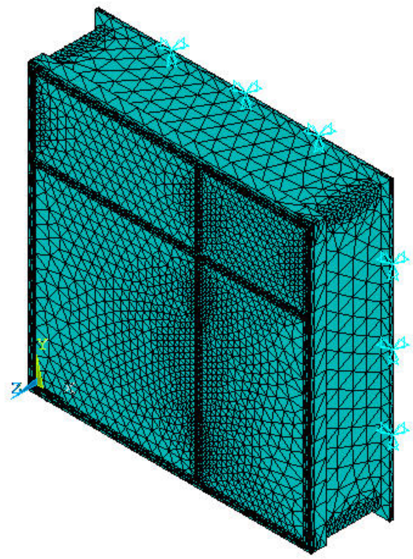

Figure 3.12 – FEA model of the GRID-LOCK® test structure

Table 3.3– Material properties used in the FEA

Material	Young's modulus (GPa)	Poisson's ratio	Density (kg/m^3)
Aluminum	66.0	0.33	2700.0
Epoxy	5.0	0.31	1500.0

Modal analysis of the FEA model revealed natural frequencies that closely matched experimental results (Table 3.4). Because disbond is a separation of adhesive and adherend that creates two traction-free surfaces, it was simulated in the FEA model by removing a 50 mm segment of epoxy at the same location where it was experimentally induced (Figs. 2, 7). The Mode 1 results of Table 3.4 are highly accurate, as FEA is known to have less model uncertainty (associated with unmodeled dynamics, non-linearities, parametric uncertainties, etc.) at lower frequencies. Results associated with higher modes, particularly Mode two, do not correlate as well with the experimental data. The trend, however, is consistent: disbond failure tends to reduce natural frequencies both in experiment and simulation.

Next, an internal pressure of 138 kPa was simulated to determine nodal displacements of the FEA model (perpendicular to the top surface) before and after disbond. Figure 3.13 shows simulated displacements for locations above internal joints. Simulated displacements (before and after disbond) compare favorably with experimental measurements (Figure 3.10) and clearly indicate the presence of disbond. The peak experimental displacement (0.25 mm directly above disbond) was only 12.0% greater than the simulated peak displacement (0.22 mm).

Table 3.4– FEA and experimental natural frequency comparison

Mode	Natural Frequencies (Hz)					
	Before Disbond		After Disbond		Change (%)	
	Experiment	FEA	Experiment	FEA	Experiment	FEA
1	1186.2	1189.4	1167.0	1171.8	-1.6	-1.4
2	1326.4	1329.1	1299.2	1327.2	-2.0	-0.1
3	2127.9	2040.6	2049.5	1868.3	-3.6	-8.4

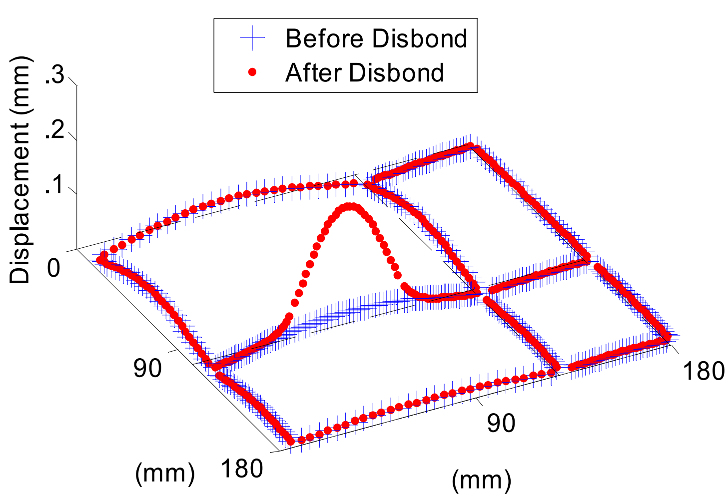

Figure 3.13 – FEA nodal displacements for internal pressure of 138 kPa before and after disbond

Additional simulations were conducted using this validated FEA model to investigate the effectiveness of these NDE techniques on less severe damage mechanisms. Epoxy cohesive strength reduction, for example, could result from service-induced defects (yielding, corrosion, etc.) or improper manufacturing procedures (inadequate surface preparation, epoxy cure time, etc.). To simulate this damage mechanism, the Young's modulus of epoxy along the joint segment where disbond was experimentally induced (50 mm in length) was reduced by 20.0% (from 5.0 GPa to 4.0 GPa). Modal analysis of the FEA model revealed no significant changes in natural frequencies associated with this simulated damage (Table 3.5). This result indicates that epoxy strength reduction may not lead to experimentally measurable changes in natural frequency; hence vibration-based damage detection might not be effective in detecting such damage mechanisms.

Table 3.5 –FEA natural frequencies before and after simulated damage (change in epoxy stiffness along 50 mm joint length)

Natural Frequency (Hz)	Young's Modulus of Epoxy (GPa)		Change (%)
	5.0	4.0	
1	1189.4	1189.2	-0.01
2	1329.1	1329.1	0.00
3	2040.6	2040.3	-0.01

Simulations involving internal pressurization (138 kPa) revealed that nodal displacements directly above the weakened joint (Figure 3.14) changed only slightly with damage (peak difference of 0.7 μm). However, skin displacements in regions adjoining the weakened joint segment (Figure 3.13) were more strongly correlated to damage (peak difference of 18.0 μm). These results suggest that optical inspection of GRID-LOCK® structures could be effective in detecting such damage mechanisms. Potential approaches for large surfaces might include optical holographic or full-field measurement techniques [26].

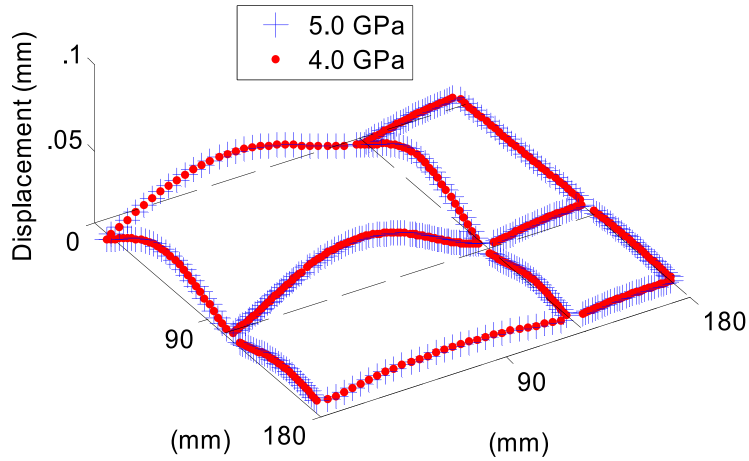

Figure 3.14 – FEA nodal displacements for internal pressure of 138 kPa before and after simulated damage (change in epoxy stiffness along 50 mm joint length)

3.6 Conclusions

Different damage detection methods were experimentally investigated for a customized GRID-LOCK® test structure. A joint disbond of substantial size (50 mm length) was induced in the test structure by utilizing an inferior epoxy and loading with internal air pressurization. The disbond was not evident in an ultrasonic C-scan (Figure 3.7), indicating that ultrasonic inspection is not a viable inspection method for GRID-LOCK® structures. Vibration-based damage detection (Figures 3.8 and 3.9) and optical displacement measurements (Figure 3.10) both successfully indicated the presence of disbond. Only the latter, however, could be used to approximate the extent and location of damage. FEA revealed that the latter method has an additional advantage. Strength loss in epoxy does not significantly alter natural frequencies (Table 3.5) but produces significant changes in structural deformation (Figure 3.15). These advantages make optical displacement measurements a feasible technique for in-service inspection and production quality control of GRID-LOCK® structures. To enhance the feasibility of this approach for large GRID-LOCK® structures, future research will investigate full-field measurement techniques such as optical interferometry and holography.

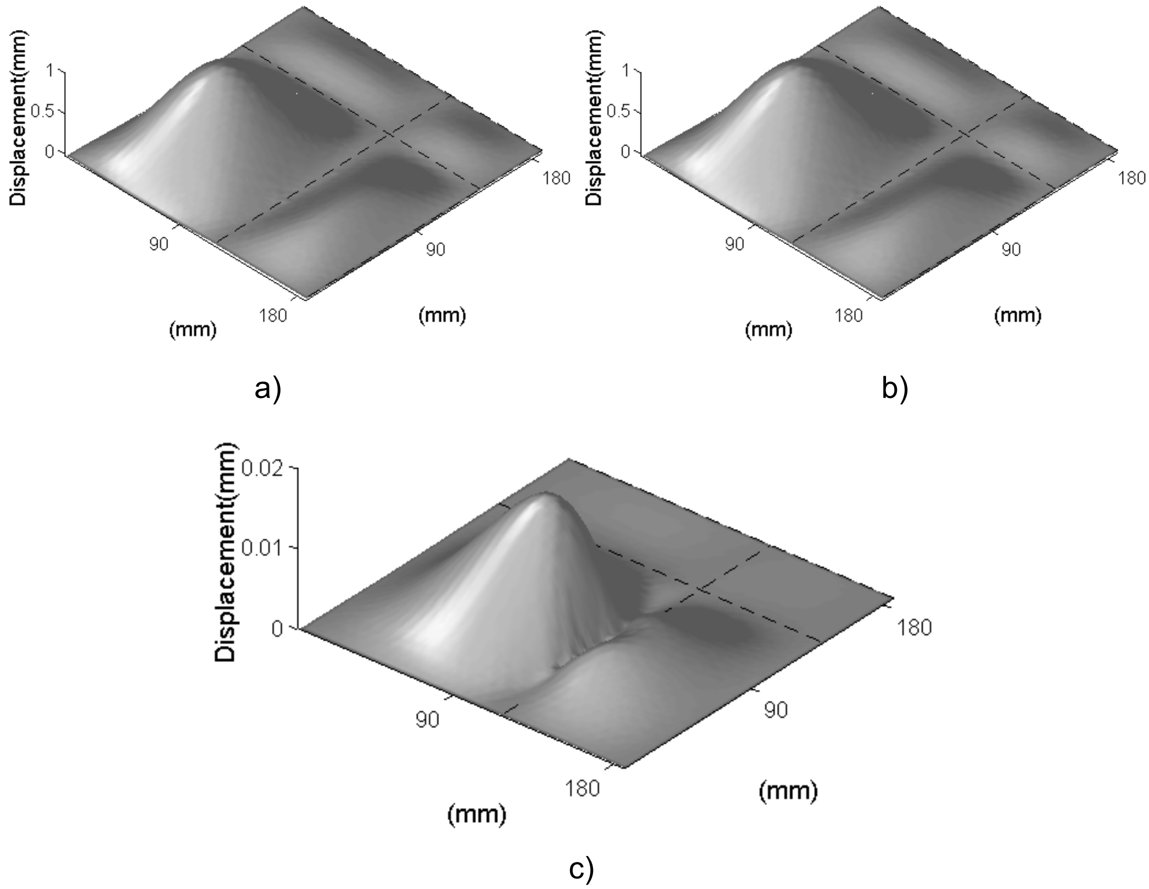

Figure 3.15 – Nodal displacements for internal pressure of 138 kPa:
a) before simulated damage, b) after simulated damage, c) net change

Acknowledgements

The authors would like to thank the Goodrich Corporation for funding this research. The authors also thank David Motley and Clinton Salter of the Cherry Point Naval Aviation Depot for performing the ultrasonic C-scans.

References

[1] S. J. Peter, Nondestructive Evaluation: Theory, Techniques, and Applications. Marcel Dekker Inc, New York, USA, 2002.

[2] C.J. Staszewski, C. Boller, G.R. Tomlinson, Aircraft Structural Health and Usage Monitoring, Health Monitoring of Aerospace Structures: Smart Sensor Technologies and Signal Processing, John Wiley and Sons, Chichester, West Sussex, England, 2004.

[3] A. Sophian, G.Y. Tian, D. Taylor, J. Rudlin, Design of a pulsed eddy current sensor for detection of defects in aircraft lap-joints, Sensors and Actuators, A: Physical, 101(1-2) (2002) 92-98.

[4] D.K. Hsu, T.C. Patton, Development of ultrasonic inspection for adhesive bonds in aging aircraft, Materials Evaluation, 51(12) (1993) 1390-1397.

[5] W.L. Dunn, A.M. Yacout, Corrosion detection in aircraft by X-ray backscatter methods, Applied Radiation and Isotopes, 53(4) (2000) 625-632.

[6] W. Jueptner, T. Bischof, Investigation of fiber reinforced plastics based components by means of holographic interferometry, in: Proceedings of SPIE - The International Society for Optical Engineering, Vol.1400, 1991, pp. 69-79

[7] http://www.aerostructures.goodrich.com/html/gridlock.asp, Goodrich Corporation Aerostructures group, 850 Lagoon Drive, Chula Vista, California 91910-2098, USA.

[8] Jason Smith, F-15, Flying Safety magazine - U.S Department of the Air Force, 59(1-2) (2003) p18-20.

[9] Jason Smith, F-15, Flying Safety magazine - U.S Department of the Air Force, 60(1-2) (2004) p11-13.

[10] R.B. Heslehurst, Observations in the structural response of adhesive bondline defects, International Journal of Adhesion and Adhesives, 19, 1999, 133-154.

[11] R.D. Adams, J. Comyn, W.C. Wake, Structural adhesive joints in engineering, Second edition, Chapman & Hall, London, England, 1997.

[12] C.V. Subramanian, M. Thavasimuthu, P. Palanichamy, D.K. Bhattacharya, B. Raj, Evaluation of bond integrity in sandwiched structures by dry couplant ultrasonic technique , NDT International, 24(1) (1991) 29-31.

[13] D.R. Motley, Analysis of low velocity impact on pultruded fiber reinforced polymer plates, M.S. Thesis, Department of Mechanical and Aerospace Engineering, North Carolina State University, Raleigh, 2002.

[14] P.E. Carden, P. Fanning, Vibration Based Condition Monitoring: A Review. Structural Health Monitoring, 3(4) (2004) 355-377.

[15] S.W. Doebling, C.R. Farrar, M.P. Prime, Summary Review of Vibration Based Damage Identification Methods. Shock and Vibration, 30(2), 1998 91- 105.

[16] P. Verboven, E. Parloo, P. Guillaume, M. Van Overmeire, Autonomous Structural Health Monitoring - Part I: Modal Parameter Estimation and Tracking, Mechanical Systems and Signal Processing, 16(4) (2002) 637-657.

[17] K. Worden, G. Manson, D. Allman, Experimental Validation of a Structural Health Monitoring Methodology. Part II. Novelty Detection on a Gnat Aircraft, Journal of Sound and Vibration, 259(2) (2003) 345-363.

[18] P.D. Samuel, D.J. Pines, A Review of Vibration-based Techniques for Helicopter Transmission Diagnostics, Journal of Sound and Vibration, 282 (1-2) (2005) 475-508.

[19] P. Rastogi , D. Inaudi, Trends in optical non-destructive testing and inspection, Elsevier, New York , 2000.

[20] R. Ambu, F. Aymerich, F. Ginesu, P. Priolo, Assessment of NDT interferometric techniques for impact damage detection in composite laminates, Composites Science and Technology, 66(2) (2006) 199-205.

[21] P. Hariharan, Optical holography: principles, techniques, and applications, Cambridge University Press, New York, 1986.

[22] P.W. Peters, M.A. Sutton, W.F. Ranson, W.P. Poplin, D.M. Walker, Whole-field experimental displacement analysis of composite cylinders, Experimental Mechanics, 29(1) (1989) 58-62.

[23] Annual book of ASTM standards, Section. 15, Vol. 15.06, 1999.

[24] F. Vestroni, D. Capecchi, Damage detection in beam structures based on frequency measurements, Journal of Engineering Mechanics, 126(7) (2000) 761-768.

[25] N.M.M. Maia, J.M.M. Silva, E.A.M. Almas, R.P.C. Sampaio, Damage detection in structures: From mode shape to frequency response function methods, Mechanical Systems and Signal Processing, 17(3) (2003) 489-498.

[26] D. Lecompte, J. Vantomme , Crack Detection in a Concrete Beam using Two Different Camera Techniques, Structural Health Monitoring, 5(1) (2006) 59-68.

4 Defect Identification in GRID-LOCK® Joints

Abstract

Damage detection in aircraft structures is conducted using a variety of non-destructive evaluation (NDE) techniques, including visual inspection, ultrasonic inspection, eddy current inspection, radiography and optical methods. These techniques are well established and have distinct advantages and limitations. Optical NDE methods show significant promise for variety of aerospace structural components, including inspection of bonded metallic GRID-LOCK® structures. In this paper, a full-field surface slope measurement technique (shearography) is utilized to confirm the effectiveness of optical NDE. Two bond defects (one disbond and one weak bond) are incorporated into a GRID-LOCK® test structure and internal pressurization results in *qualitative* indications of damage on the shearograms. Because accurate characterization of structural defects is critical to flight safety, a *quantitative* non-destructive evaluation (QNDE) method using a scanning optical probe is also explored. This QNDE method involves use of radial basis function networks (RBFNs) trained and validated using FEA nodal displacements.

Keywords: GRID-LOCK® structures; optical non-destructive evaluation; shearography; surface displacement measurement; artificial neural networks; radial basis function network

4.1 Introduction

Non-destructive evaluation (NDE) of aerospace structures can be conducted using variety of well-established techniques including visual inspection, ultrasonic inspection, eddy current inspection, radiography and various optical methods [1]. Each technique has distinct advantages and limitations [2]; the suitability of each approach for a particular structure is determined from the structure's physical characteristics (geometry, materials, accessibility, etc.) and the evaluation objectives. While inspection methods for certain conventional structures (such as ultrasonic c-scan inspection of honeycomb panels [3] and composites plates [4]) have matured, emerging lightweight construction methods necessitate the development of advanced and customized inspection methods.

One such aircraft structure is the GRID-LOCK® technology recently developed by the Goodrich Corporation. GRID-LOCK® is an innovative method of joining structural components with simple tongue and groove joints (Figure 4.1). The simplest GRID-LOCK® structure consists of two precision-machined metal parts: a base with integral ribs and a cover with integral grooves. The ribs of the base mate with the grooves of the cover and the joint is formed by an epoxy. Multi-directional ribs are machined in the base resulting in a cellular type construction. The result is a structurally efficient, double-skinned, ribbed-core structure that is approximately twice as strong and stiff as a stiffened-skin or isogrid structure of equal weight [5].

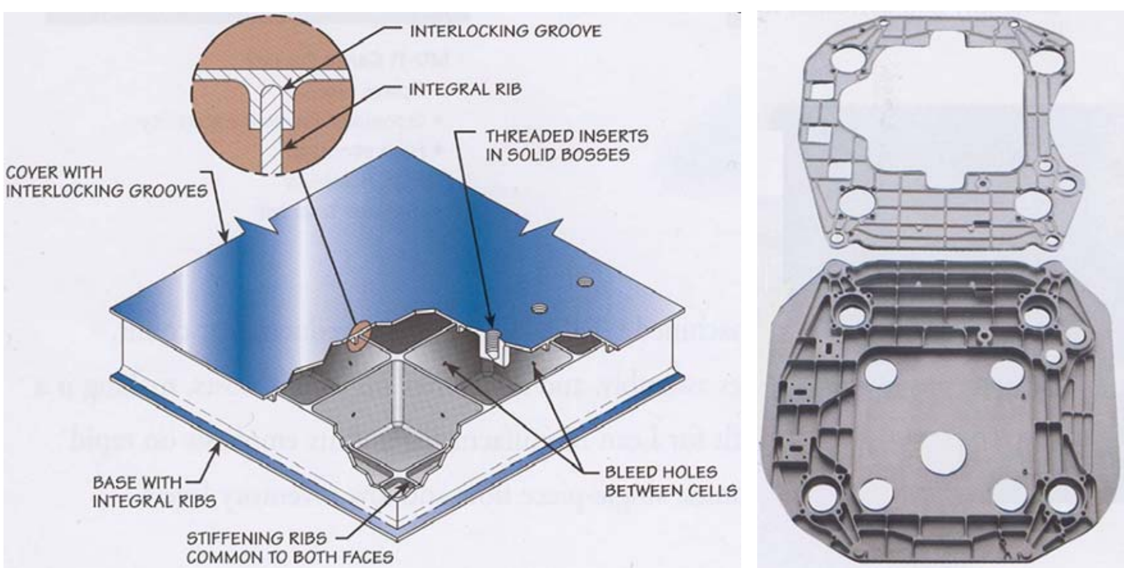

a) b)

Figure 4.1- GRID-LOCK® structures: a) Basic construction,
b) Components of an AV-8B Harrier bulkhead

GRID-LOCK® structures are ideally suited to a variety of commercial, military and space applications. Recently, they have replaced honeycomb structures located on the horizontal stabilator of the F-15E fighter aircraft [6]. These structures experience extreme loading conditions in harsh operating environments, and a limited number of base and cover separation failures have been reported [7]. Advanced NDE techniques are needed to inspect the internally bonded joints of GRID-LOCK® structures and prevent such failures. The primary difficulty associated with inspection is that once assembled, accessibility to the interior is severely restricted. Permanent sensor placement for continuous monitoring is not viable considering the harsh operating environments of these structures.

Previously [8], the authors established by means of experimental investigations and finite element analysis (FEA) that optical NDE (with internal pressure loading) is superior to vibration-based damage detection and ultrasonic C-scan inspection for detecting GRID-LOCK® bond defects. Optical inspection was accomplished using point-by-point displacement measurements, a tedious process that may not be suited for practical implementation on large aircraft structures. In this paper, a full-field surface slope measurement technique (shearography) [9] is utilized to confirm the effectiveness of optical NDE. Two bond defects (one disbond and one weak bond) are incorporated into a GRID-LOCK® test structure and internal pressurization results in *qualitative* indications of damage on the shearograms. Because accurate characterization of structural defects is critical to flight safety, a *quantitative* non-destructive evaluation (QNDE) [10] method using a scanning optical probe is also explored. This QNDE method involves use of artificial neural networks (ANNs) [11] trained and validated using FEA nodal displacements.

4.2 Background

Optical NDE methods [12] involve the use of light and its reflective properties to identify surface and sub-surface defects in structures. Typically optical NDE is accomplished using interferometric techniques [13] (Moiré interferometry, holography, etc.) as they enable rapid and accurate inspection of large surfaces. These techniques monitor surface deformations of a loaded structure; structural defects can be correlated to changes in these measurements. One among these techniques is shearography [14, 15], a method that can be used to measure the out-of-plane displacement gradient or slope. In this technique, a reference image and a sheared image (offset by angle and displacement) of a test object are produced using a laser light source (Figure 4.2). These images are made to interfere and form a speckle pattern on a CCD video camera. Several laser speckle patterns (produced by introducing different phase shifts between interfering beams) are formed and utilized to calculate pixel-by-pixel phase values. The procedure is repeated after slightly deforming the test object. The phase differences obtained by subtracting the two sets of pixel-by-pixel phase values can be solely attributed to structural deformation. Hence, these values can be used to calculate surface slopes along the directions of image shear. Generally, defect-induced local slope patterns differ from the global slope patterns and hence defect locations can be discerned. Various methods can be used to deform the test object; these include vacuum and pressurization loading, mechanical vibration, and thermal expansion.

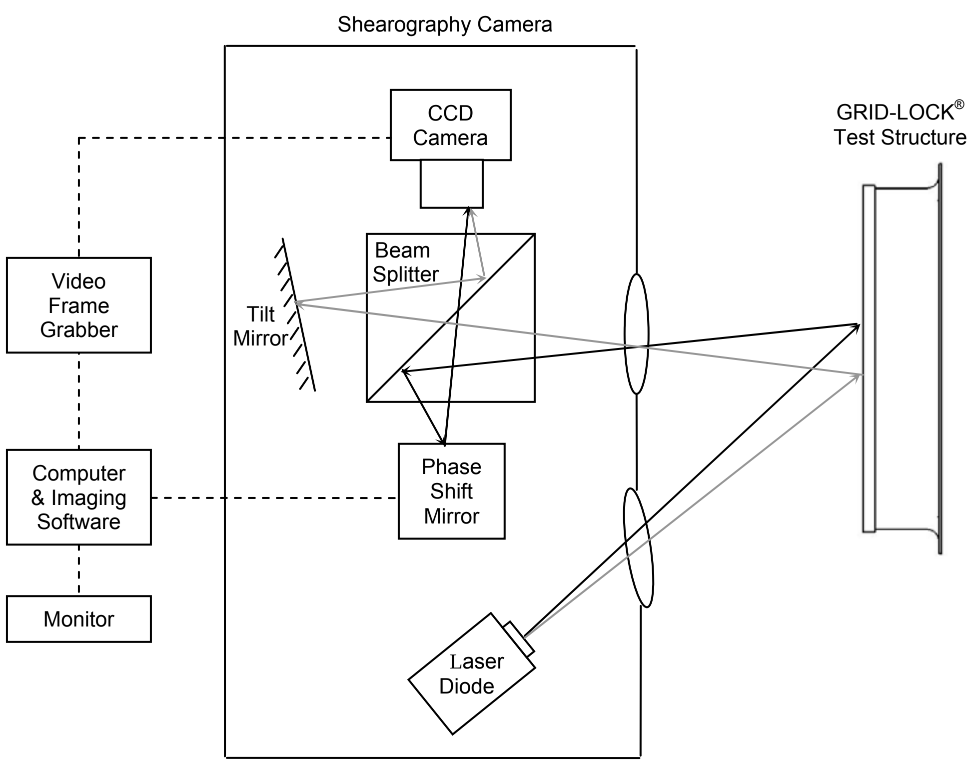

Figure 4.2 – Layout for laser shearography [16]

Quantitative non-destructive evaluation (QNDE) refers to the detection and characterization of defects in a structure in order to prevent failure. In recent years, techniques using artificial neural networks (ANNs) [17,18] have shown significant promise for QNDE because of their excellent pattern recognition capabilities. ANNs are highly interconnected data processing elements (neurons) capable of modeling any nonlinear mapping to any desired level of accuracy. Because they must be trained before they can be used as a tool for QNDE, training is carried out using a set of experimentally measured or simulated inputs (vibration parameters [19], static displacements [20], acoustic emission signals [21], etc.) and target outputs (defect type, size, location, etc.). During training, network parameters (network weights, number of neurons, etc.) are adjusted by a learning algorithm until the network outputs are within a specified tolerance (error goal) of the target outputs. Validation is usually performed with input/output data not used during the training phase to ensure that adequate network generalization has occurred.

Although a variety of ANN architectures have been explored previously for QNDE, the radial basis function network (RBFN) provides an effective, accurate, and localized approach [22, 23]. The RBFN (Figure 4.3) consists of an input layer, a hidden layer of radial basis function (RBF) neurons and a linear output layer. Each RBF in the hidden layer is defined by a center (the midpoint of the RBF with respect to an input variable), a distribution (the "spread" of the RBF), and a weight (the amplitude of the RBF). The hidden layer neurons are most affected by localized portions of the input vector space, making them ideally suited to the task of interpreting displacement information to determine the existence, location, and severity of joint defects in GRID-LOCK® structures.

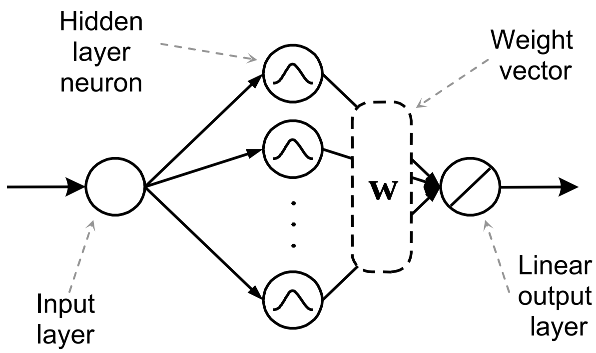

Figure 4.3 – Typical RBFN architecture

4.3 Methods and Materials

4.3.1 Test Structure Fabrication

The experimental study required the design and fabrication of a GRID-LOCK® test structure (Figures 4.4 and 4.5). This specimen was designed to incorporate the prominent features of GRID-LOCK® structures: cellular construction with epoxy-bonded tongue and groove joints. The test structure features four cells of equal dimensions, resulting in four internal joint segments (numbered 1 - 4 in Figure 4.4). The base of this test structure features a lip for securing the specimen during pressurization and displacement measurement. A Schrader valve was fitted to one of four cells for internal pressurization, and small bleed holes in the internal partitions facilitated the distribution of air to each cell. This test specimen was machined out of 6061 aluminum using a Haas VF-1 CNC milling machine.

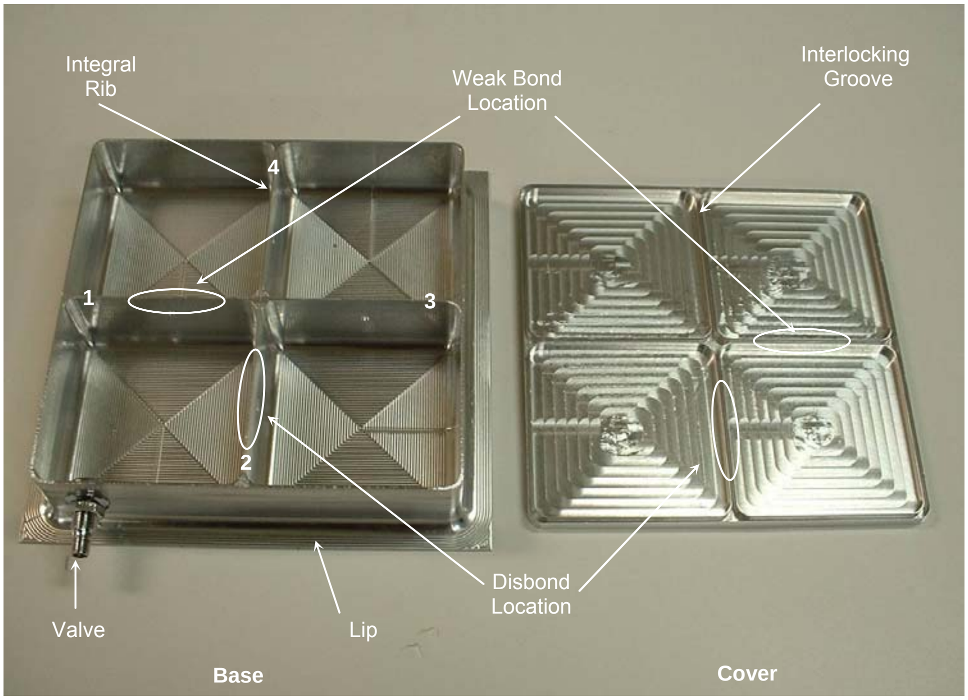

Figure 4.4 - Base and cover of the GRID-LOCK® test structure before bonding

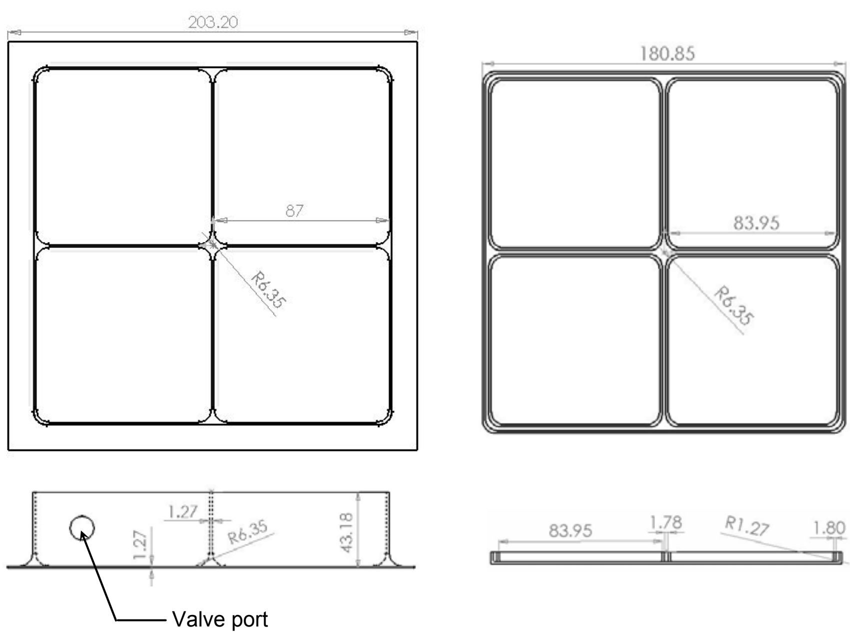

Figure 4.5 - Dimensions of GRID-LOCK® test structure (mm): a) base b) cover

Before bonding, the faying surfaces were abraded and cleaned with Methyl Ethyl Ketone (MEK). Two bond defects, a weak bond (low strength, flexible two-part epoxy 3M® DP- 105) and a disbond (no epoxy) of same length (25 mm), were incorporated into the test structure near the midpoints of two internal joint segments (1 and 2). The remaining joint portions were bonded with a high strength two-part epoxy (3M® DP- 460). The published shear strength (ASTM D 1002) [24]) of the low strength and high strength epoxies are 10342 kPa and 31000 kPa, respectively. The adhesives were then cured at room temperature (24°C) for a period of 48 hr.

4.3.2 Laser Shearography Experiment

Laser shearography measurements of the test structure (Figure 4.6) were carried out at Laser Technology, Inc. of Norristown, PA [25]. The top surface of the specimen was imaged using a LTI-5100 Digital Shearography Camera for an internal pressure of 55.0 kPa. In-plane image shearing (5.08 mm displacement) was performed along the orthogonal axes of the specimen's top surface (X and Y in Figure 4.6). Shearograms representing out-of-plane displacement gradients $\left(\frac{dZ}{dX}\right)$ and $\left(\frac{dZ}{dY}\right)$ were produced from the digitized images.

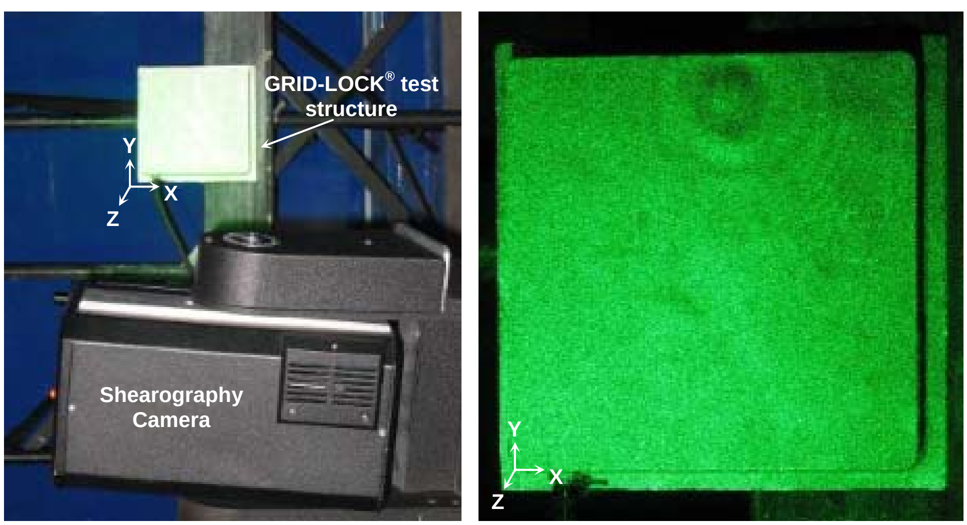

a) b)

Figure 4.6 – a) Laser shearography test setup b) GRID-LOCK® test structure illuminated by laser

4.3.3 Surface Displacement Measurements

Surface displacements of the specimen's top surface were also measured using a custom-built optical scanning system (Figure 4.7). The principle components of this scanning system included a CNC XY table (from a Sherline Model 2000 vertical milling machine) and a non-contact fiber optic displacement sensor (Philtec RC-89). A National Instruments PCI-6024E multi-function data acquisition (DAQ) card and xPC Target™ software were used for the data acquisition. The lip on the test structure base was clamped to the XY table and the displacement sensor was mounted on an articulated arm. The XY table was then programmed to follow a raster pattern consisting of 144 lines in the Y direction (1.27 mm spacing between lines) at a feed rate of 7.62 mm/s. This allowed the displacement sensor to scan the entire 182.8 mm × 182.8 mm area of the test structure. To ensure that deflection measurements were properly registered with X and Y locations, data acquisition of the displacement signal was triggered to the feed axes of the XY table. For this purpose, a laser tachometer (Monarch PLT 200) was focused on a reflecting strip attached to the Y-axis cross feed handle. The handle rotated once for every 1.27 mm of table travel in the Y direction, resulting in a voltage pulse output from the tachometer every 1.27 mm. This pulse was used to trigger data acquisition from the optical displacement sensor. At each trigger, averages of 10 consecutive measurements (acquired at a sampling frequency of 1000 Hz) were recorded. Thus a 1.27 mm × 1.27 mm measurement resolution was achieved during surface scanning.

It should be noted that during scanning the test structure boundary conditions were asymmetric; only lips along two sides could be clamped to the XY table. Therefore two scans at an internal pressure of 138 kPa were performed. The first scan was done with joint segments 1 and 3 being parallel to the X-axis and the second one with joints 2 and 4 being parallel to the X-axis (Figure 4.7).

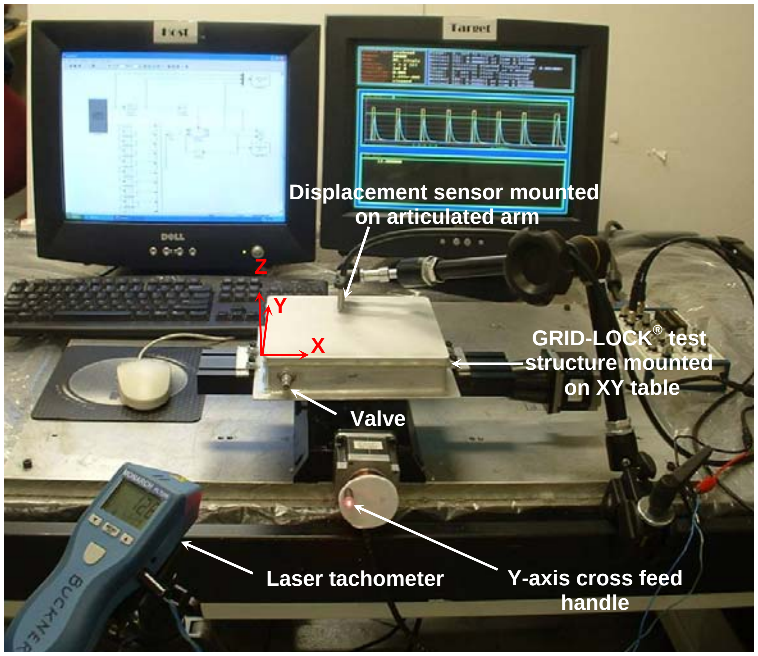

Figure 4.7 – Set up for surface displacement measurement

4.3.4 Defect Identification using Radial Basis Function Networks

RBFNs for defect identification were designed using functions available in the MATLAB® neural network toolbox [26]. Specifically, the *newrb* function (which uses an orthogonal least squares learning algorithm [27] for training) was used to facilitate QNDE. This tool adds one RBF neuron to the hidden layer following each training iteration (epoch). The centers of these neurons are equal to input vectors that produce maximum reduction in network error. This process is carried out until the specified error goal (mean squared error between target outputs and network outputs) is met.

The RBFN utilized for defect identification in the GRID-LOCK® test structure had 28 displacement inputs. These values were sub-sampled from the overall surface displacement measurements and were extracted from areas directly above the mid-plane of internal joint segments (Figure 4.11). The two RBFN outputs were defect length (mm) and centroid location in the joint segment of interest. RBFN training (Figure 4.8a) and validation (Figure 4.8b) was accomplished using FEA nodal displacements corresponding to various defect simulations. RBFN testing (Figure 4.8c) was done using subsets of experimentally generated displacements.

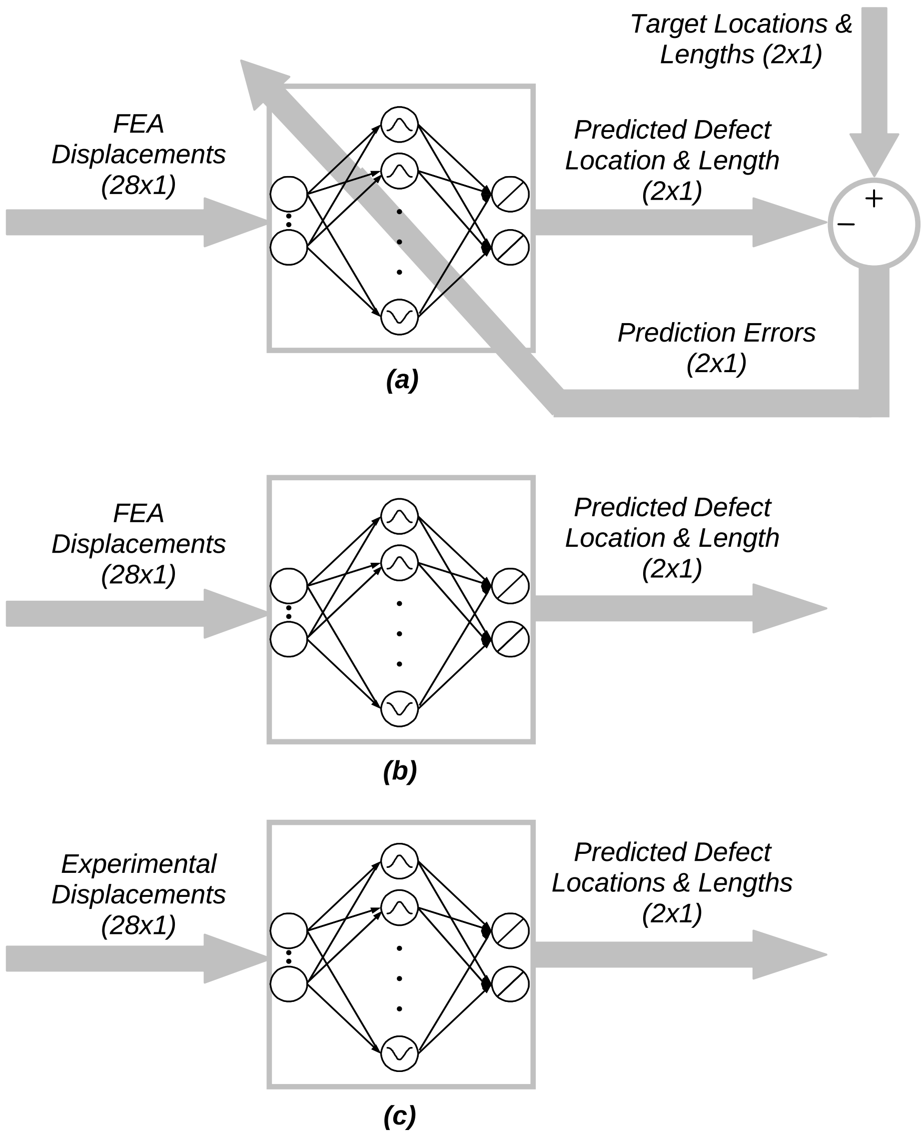

Figure 4.8 - RBFN phases (a) Training, (b) Validation, and (c) Testing

4.3.5 Finite Element Analysis

RBFN training and validation cases were generated from a finite element model of the GRID-LOCK® test structure. The FEA model was developed in ANSYS® using a total of 13,156 ten-node SOLID92 elements. Only one of the four test structure cells was modeled, taking advantage of specimen symmetry (Figure 4.9) and reducing computational overhead. All degrees of freedom for nodes along the clamped lip portions in experiment (Figure 4.7) were constrained and symmetry boundary conditions were applied along symmetry planes. The material properties used in the model are listed in Table 4.1. Accuracy of the FEA model was established by comparing the simulated peak skin displacement resulting from an internal gauge pressure of 138.0 kPa (1.10 mm) to the peak experimental skin measurement (over all four test structure cells at same internal pressure… 1.06 mm).

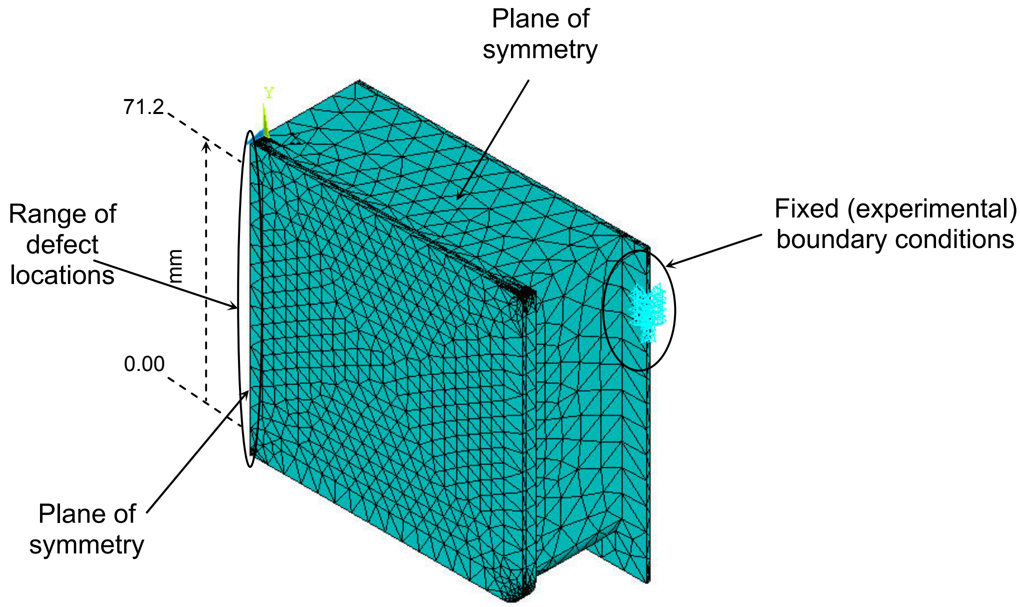

Figure 4.9 – FEA model of quarter GRID-LOCK® test structure

Table 4.1 – Material properties used in the FEA

Material	Young's modulus (GPa)	Poisson's ratio	Density (kg/m^3)
Aluminum	66.0	0.33	2700.0
Epoxy	5.0	0.31	1500.0

A total of 22 simulations were conducted using this FEA model for an internal pressurization of 138.0 kPa. One simulation was done with no defect and the rest were done after inducing defects (of different length and location) along one internal joint segment, as illustrated in Figure 4.9. All of the defects induced corresponded to a 99.99 % reduction in the Young's modulus of the epoxy. Table 4.2 lists the defect lengths and centroidal locations (along a 0-71.2 mm internal joint length shown in Figure 4.9) for the various simulation cases. After each simulation, nodal displacements directly above the joint segment were extracted.

Table 4.2 – Simulated joint defect lengths and centroidal locations

Defect Number	Centroid Location (mm)	Defect Length (mm)
1	N/A (No Defect)	N/A (No Defect)
2	27.0	38.1
3	31.8	38.1
4	35.0	38.1
5	39.0	38.1
6	42.6	38.1
7	47.0	38.1
8	50.9	38.1
9	25.4	28.6
10	29.4	28.6
11	32.6	28.6
12	37.0	28.6
13	40.6	28.6
14	45.0	28.6
15	50.2	28.6
16	22.3	19.0
17	27.8	19.0
18	32.2	19.0
19	36.6	19.0
20	40.2	19.0
21	43.4	19.0
22	54.2	19.0

4.4 Results

4.4.1 Laser Shearography

The 25 mm weak bond (located in joint segment 1) was clearly visible in the shearogram developed with image shearing in the X direction (Figure 4.10 a). Similarly, the 25 mm disbond (located in joint segment 2) was clearly visible in the shearogram with image shearing in the Y direction (Figure 4.10 b).

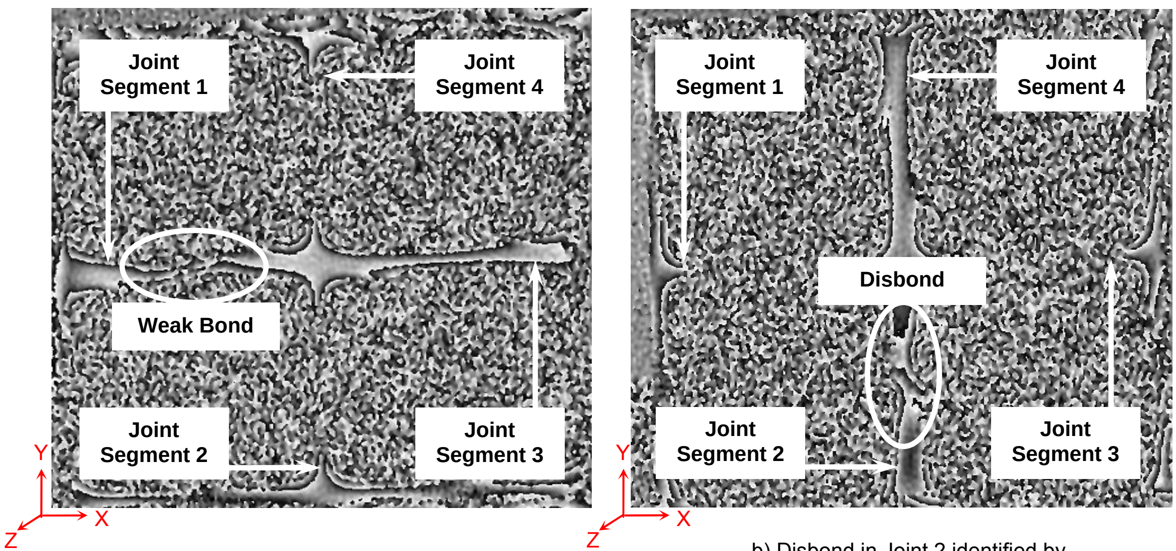

a) Weak bond in Joint 1 identified by image shearing along X direction

$$\left(\frac{dZ}{dX}\right)$$

b) Disbond in Joint 2 identified by image shearing along Y direction

$$\left(\frac{dZ}{dY}\right)$$

Figure 4.10 – Bond defects identified in shearograms

Both shearograms were obtained at a gauge pressure of 55.0 kPa, which produced excessive skin displacements over the test structure cells. These displacements were so high that they exceeded the resolution capabilities of the shearography camera and produced image de-correlation over the four cells. The de-correlations over joint segments oriented perpendicular to direction of shearing (e.g. segments 2 and 4 in Figure 4.10a) occur because the magnitude of shearing

(5.08 mm) caused skin regions to be superimposed over joint regions. It is worth noting the smooth, uninterrupted nature of joint segments adjacent to the bond defects in Figure 4.10, indicating regions of zero slope with no corresponding defects.

4.4.2 Surface Displacement Measurements

Figure 4.11 shows selected results from the optical scanning experiments. This surface plot represents the skin deflections resulting from an internal gauge pressure of 138.0 kPa. Because the deflections are relatively large (up to 1.06 mm), it is not possible to discern joint defects (which are predicted to have an amplitude of only 0.03 mm) from this image. Subsets of this displacement data (line scans above the joint segments, Figure 4.12) were extracted for use as inputs RBFN testing (Section 4.3.2).

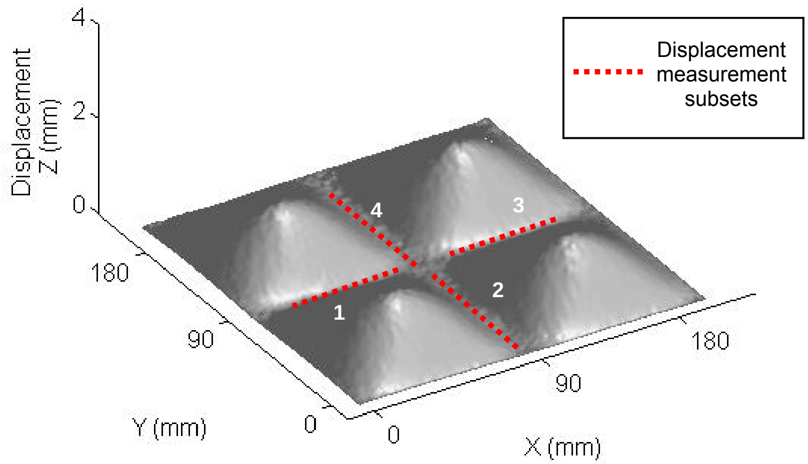

Figure 4.11 – Test structure top surface scan at an internal pressure of 138 kPa

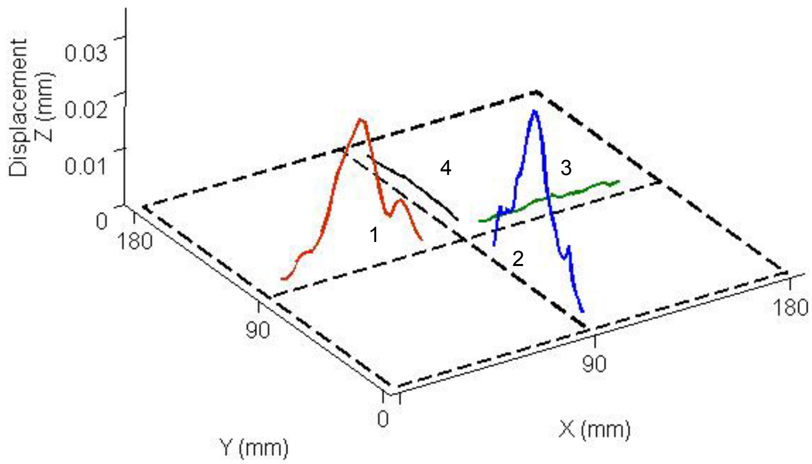

Figure 4.12 – Extracted line scans above joint segments for use with RBFN testing

It should be noted that peak displacements above the weak bond (joint segment 1, 0.025 mm peak) and disbond (joint segment 2, 0.029 mm peak) were very similar (a 16.0% difference). Subsequent FEA simulations (138.0 kPa gauge pressure) revealed that maximum epoxy Von-mises stress in the weak bond (7.5 MPa) actually exceeded the failure stress (4.1 MPa). Experimentally, this likely caused epoxy failure (disbond) instead of weak bond in joint segment 1, resulting in similar displacement values above the defect locations.

4.4.3 Defect Identification using Radial Basis Function Networks

Before RBFN training and validation, FFT magnitudes of the FEA simulation data (all 22 cases described in Section 3.4) and experimental measurements (line scans extracted from above the joint segments shown in Figure 4.12) were plotted to compare spatial frequency information. From this comparison, it was noted that low-amplitude, high-frequency components (associated with optical reflection and electrical noise) were present in experimental data. Hence, band-limited white noise (amplitude 1.5 10^{-3} mm) was added to the FEA data to make it resemble the experimental data. Figure 4.13 shows the resulting comparison FFT magnitudes comparison between FEA simulation and experimental data.

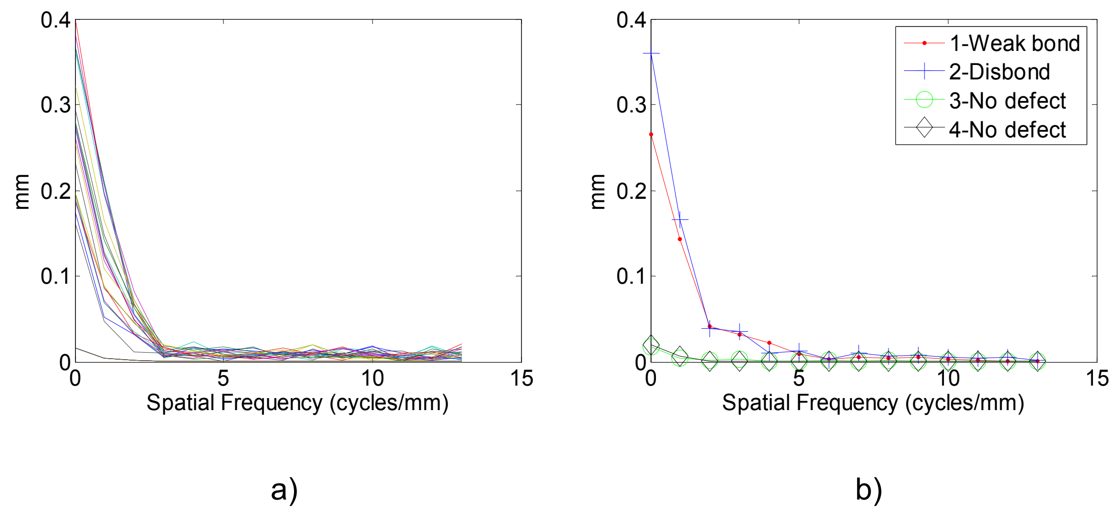

Figure 4.13- FFT of displacement data a) FEA after noise addition b) Experimental

Although only one healthy (defect-free) case was simulated using FEA, several healthy cases were required for RBFN training. Six additional "healthy datasets" were generated by adding band-limited white noise (amplitude 1.5×10^{-3} mm) to the FEA data, resulting in a total of 28 training and validation cases (six healthy, 22 defective). During training the target outputs for these healthy cases were; 0 for location and 0.2 mm for length.

Of the 28 datasets, half were randomly selected for training purposes, half were reserved for validation purposes. Each dataset was sub-sampled to provide 28 displacements inputs and a corresponding target defect location and length (Figure 4.14). During training the mean squared error between target outputs and network outputs steadily decreased (Figure 4.15), reaching 6.2×10^{-18} mm^2 at the 14th epoch.

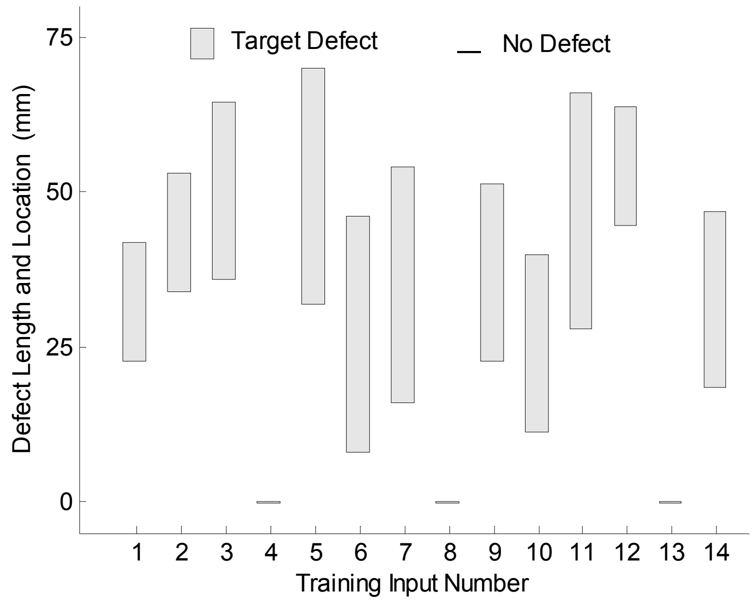

Figure 4.14– Target outputs used for RBFN training

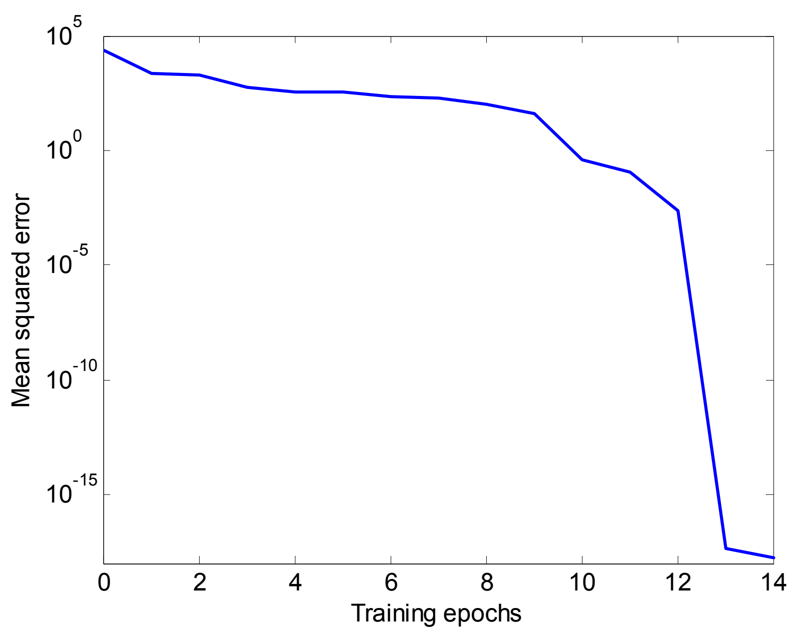

Figure 4.15 –Cost function decrease during RBFN training

After training, the remaining 14 FEA datasets were used for RBFN validation. The validation results are presented graphically in Figure 4.16, where each light gray bar represents a target defect, each dark gray bar represents an RBFN estimation of the defect, and the blackened regions represent correlation between the two. These results indicate that the trained RBFN provides reasonable estimates of the existence, location, and size of simulated defects in the GRID-LOCK® test structure.

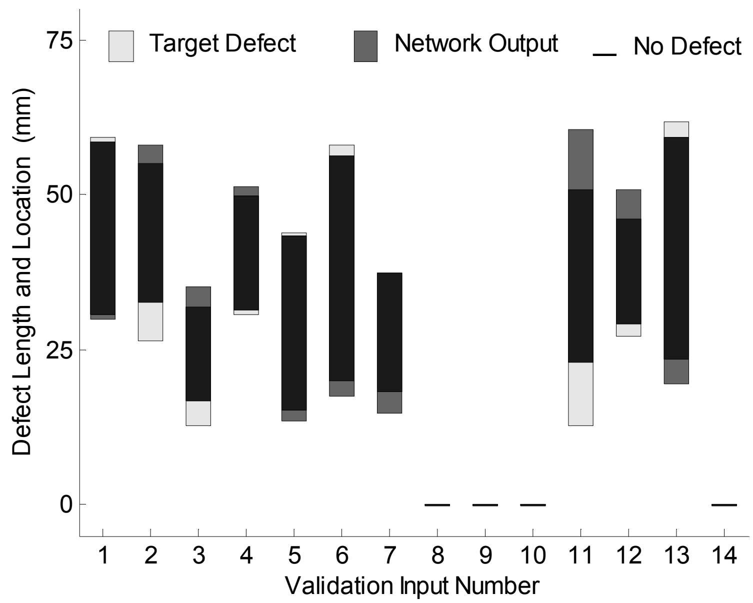

Figure 4.16 – Target and network outputs during RBFN validation

After training and validation, optical displacement scans from each of the four internal joint segments (Figures 4.11 and 4.12) were applied to the RBFN. The resulting network outputs are shown in Figure 4.17, where each light gray bar represents a target defect, each dark gray bar represents an RBFN estimation of the defect, and the blackened regions represent correlation between the two. These experimental results indicate that the trained RBFN provides reasonable estimates of the existence, location, and size of actual defects in the GRID-LOCK® test structure. The estimation errors presented in Table 4.3 further quantify the effectiveness of this defect identification approach.

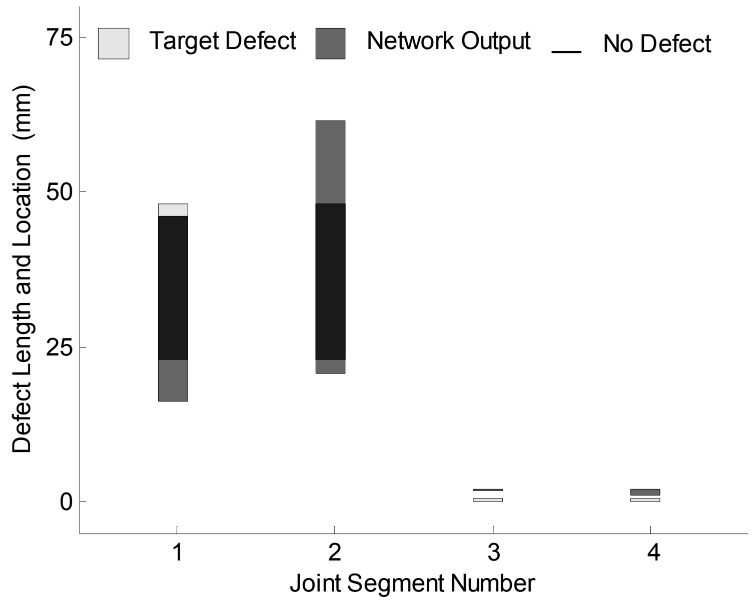

Figure 4.17 –RBFN testing results

Table 4.3 – Comparison between target and RBFN testing outputs

Joint segment number	Targets (mm)		RBFN Outputs (mm)		RBFN Prediction Errors (mm)	
	Length	Centroid	Length	Centroid	Length	Centroid
1 (Weak bond)	25.0	35.5	29.8	31.0	4.8	-4.4
2 (Disbond)	25.0	35.5	40.5	41.1	15.5	5.6
3 (No Defect)	0.2	0.0	0.4	1.9	0.2	1.9
4 (No Defect)	0.2	0.0	1.0	1.6	0.8	1.6

4.5 Conclusions

Investigations were carried out to evaluate the effectiveness of optical methods for NDE of GRID-LOCK® joints. In the experimental phase of this investigation, a GRID-LOCK® test structure was fabricated with four internal joint segments, two of which included bond defects. The existence of these defects could be clearly identified in shearograms (out-of-plane displacement gradients) of the test structure obtained through laser shearography experiments. These result confirmed the utility of optical NDE methods for defect location identification. Further efforts focused on the development of quantitative non-destructive evaluation tools utilizing artificial neural networks (ANNs). A radial basis function network (RBFN) was trained to interpret displacement data generated from FEA and determine defect locations and lengths in test structure joint segments. When tested with experimental data, the trained network was able to accurately indicate the existence of defects in internal joint segments. Furthermore, the RBFN made excellent predictions regarding defect location and extent. These results demonstrate how ANNs can be used to interpret measured surface displacements and characterize the nature of internal joint defects in GRID-LOCK® structures.

Acknowledgements

The authors would like to thank the Goodrich Corporation for funding this research. The authors also thank John Newman (Laser Technology Incorporated, Norristown, PA) for performing the laser shearography experiments.

References

[1] Peter SJ. Nondestructive Evaluation: Theory, Techniques, and Applications. New York: Marcel Dekker Inc, 2002.

[2] Staszewski CJ, Boller C, Tomlinson GR. Aircraft Structural Health and Usage Monitoring, Health Monitoring of Aerospace Structures: Smart Sensor Technologies and Signal Processing. West Sussex, England: John Wiley and Sons, 2004.

[3] Subramanian CV, Thavasimuthu M, Palanichamy P, Bhattacharya DK, Raj B. Evaluation of bond integrity in sandwiched structures by dry couplant ultrasonic technique. NDT & E International 1991; 24(1): 29-31.

[4] Motley DR. Analysis of low velocity impact on pultruded fiber reinforced polymer plates. M.S. Thesis, Department of Mechanical and Aerospace Engineering, North Carolina StateUniversity, Raleigh, 2002.

[5] http://www.aerostructures.goodrich.com/html/gridlock.asp, Goodrich Corporation Aerostructures group, 850 Lagoon Drive, Chula Vista, California 91910-2098, USA.

[6] Smith J. F-15. Flying Safety magazine- U.S Department of the Air Force 2003; 59(1-2): 18-20.

[7] Smith J. F-15. Flying Safety magazine- U.S Department of the Air Force 2003; 60(1-2): 11-13.

[8] Pandurangan P, Buckner GD. Assessment of Damage Detection Methods in GRID-LOCK® Structures. Mechanical Systems and Signal Processing, accepted Oct 4 2006.

[9] Lianxiang Y. Recent developments in digital shearography for nondestructive testing. Materials Evaluation 2006; 64 (7): 704-709.

[10] Achenbach JD. Quantitative nondestructive evaluation. International Journal of Solids and Structures 2000; 37 (1-2): 13-27.

[11] Levin RI, Lieven NAJ. Dynamic finite element model updating using neural networks. Journal of Sound and Vibration 1998; 210 (5): 593-607.

[12] Rastogi P, Inaudi D. Trends in optical non-destructive testing and inspection. New York; Elsevier, 2000.

[13] Ambu R, Aymerich F, Ginesu F, Priolo P, Assessment of NDT interferometric techniques for impact damage detection in composite laminates. Composites Science and Technology 2006; 66(2): 199-205.

[14] Newman J. Rapid Sensitive Inspection Of Marine Composites Using Laser Shearography. Technology report - Laser Technology Incorporated 2006, www.LaserNDT.com.

[15] Michael HYY, Lianxiang Y, Shang HM. Unified approach for holography and shearography in surface deformation measurement and nondestructive testing. Optical Engineering 2003; 42 (5): 1197-1207.

[16] John Newman, Laser Shearography Inspection of Helicopter Rotor Blades, Technology report - Laser Technology Incorporated 2006, www.LaserNDT.com.

[17] Kreis T, Jueptner W. Biedermann R. Neural network approach to holographic nondestructive testing. Applied Optics 1995; 34 (8): 1407-1415.

[18] Okafor AC, Dutta A. Optimal ultrasonic pulse repetition rate for damage detection in plates using neural networks. NDT and E International 2001; 34 (7): 469-481.

[19] Oberholster AJ, Heyns PS, On-line fan blade damage detection using neural networks Mechanical Systems and Signal Processing 2006; 20 (1); 78-93.

[20] Zhao J , Ivan J, DeWolf JT. Structural damage detection using artificial neural networks. Journal of Infrastructure Systems 1998; 4 (3): 93-101.

[21] Liu N , Zhu QM, Wei CY, Dykes ND, Irving PE. Impact damage detection in carbon fiber composites using neural networks and acoustic emission. Key Engineering Materials 1999; 167-168: 43-54.

[22] Reddy R, Roopesh K , Ganguli, R. Structural damage detection in a helicopter rotor blade using radial basis function neural networks. Smart Materials and Structures 2003; 12 (2); 232-241.

[23] Saadat S, Buckner GD, Furukawa T, Noori MN. An intelligent parameter varying (IPV) approach for non-linear system identification of base excited structures. International Journal of Non-Linear Mechanics 2004; 39 (6): 993-1004.

[24] Annual book of ASTM standards, Section. 15, Vol. 15.06, 1999.

[25] Laser Technology Incorporated, 1055 W. Germantown Pike, Norristown, PA 19403 USA, www.LaserNDT.com.

[26] http://www.mathworks.com/access/helpdesk/help/toolbox/nnet/, MATLAB® neural network toolbox documentation.

[27] Chen S, Cowan CFN, Grant PM. Orthogonal Least Squares Learning Algorithm for Radial Basis Function Networks. IEEE Transactions on Neural Networks 1991; 2 (2): 302-309.

5 Conclusions

This dissertation outlined the development and assessment of nondestructive evaluation (NDE) methods for bond defect detection in GRID-LOCK® joints. The results were derived from a combination of analytical, computational, and experimental efforts. Experiments conducted using customized GRID-LOCK® test structures revealed that vibration based damage detection methods can indicate the presence of disbond, but not information regarding its location or extent. Experiments also demonstrated that optical NDE using point-by-point surface displacement measurements can indicate disbond presence, location and extent. Additional experiments involving ultrasonic C scan inspections proved ineffective due primarily to a lack of probe access to the joints.

Finite Element Analysis (FEA) was used to validate and extend the experimental investigations. FEA of an accurate GRID-LOCK® test structure revealed that weak bonds do not significantly affect vibration response. However, weak bonds cause significant changes in structural deformation that can be identified by optical measurements. The use of FEA to compare different NDE approaches avoided experimental testing on large numbers of GRID-LOCK® test structures and demonstrated how FEA can enhance the basic NDE approach.

Full-field surface imaging experiments involving shearography resulted in *qualitative* indications of bond defects. *Quantitative* non-destructive evaluation (QNDE) was achieved using artificial neural networks that input structural displacement data to determine defect nature. A radial basis function network (RBFN) trained and validated using bond defect data obtained from a FEA model accurately indicated the existence, location and extent of defects in internal joint segments when tested with experimental data.

These results demonstrate the superiority of optical NDE methods for bond defect identification in GRID-LOCK® structures, and illustrate how artificial neural networks can be used to interpret optical NDE data to characterize the nature of internal joint defects. Hence quantitative optical NDE is an ideal and feasible technique for in-service inspection and production quality control of GRID-LOCK® structures.

Appendices

A. Vibration-based Damage Detection in GRID-LOCK® Structures

The limited interior accessibility and complex internal geometries of GRID-LOCK® structures make it difficult to implement conventional NDE techniques like visual, ultrasonic, eddy current and X-ray radiography. Any sensors located inside these structures may not perform reliably because of the harsh operating environment, making it difficult to implement real time techniques like acoustic emission. Guided wave ultrasonic inspection is preferred for plate and beam type structures.

However, vibration-based damage detection (VBDD) offers a solution for inspection of GRID-LOCK® structures. This is demonstrated on a test structure, instrumented with one accelerometer and undergoing a realistic failure mode. The results show that vibration-based damage detection can ascertain the initiation and increase in level of damage in the structure.

1 Background

Vibration-based damage detection (VBDD) is a technique that is based on observing changes in modal parameters due to damage. In the past couple of decades there have been many successful demonstrations of VBDD for various applications [1] but still this technology has not been widely considered for aircraft structures. The reason for this restricted application is that many demonstrations of VBDD lack experimental validation [2-4]. Most experimental demonstrations of VBDD have used structures of simple geometries like plates [5], beams [6] and frames [7]. If the demonstrations were on structures with complex geometries they involve damage scenarios like a saw cuts [8], holes [9], added masses [10] etc. or require unreasonable access to sensor measurements [11,12]. In order to advance the application of VBDD to aircraft structures investigations involving real aircraft structures with realistic failure modes and sensor limitations needs to be done.

VBDD being a global technique does not require access to every part of the structure being inspected. VBDD can be implemented with limited equipment and sensors. Additionally, the data generated can be quickly and easily interpreted. The major disadvantages that have been associated with this technique are that modal parameters are sensitive to boundary and environmental conditions and higher vibration modes are difficult to excite. Most of these reports tend to come from the civil engineering community where testing is conducted on bridges [13] out in the open while being exposed variations in temperature, humidity etc. This difficulty can be overcome for GRID-LOCK® structures if testing is done in a controlled environment like an aircraft hangar. Civil structures are of an entirely different scale than aircraft structures. The smaller sizes of aircraft structures make it possible to excite more fundamental modes.

2 Experiment

An experimental investigation was done in order to determine the feasibility of using VBDD for inspection of GRID-LOCK® structures. A GRID-LOCK® test structure was fabricated (Figure A.1), constrained (Figure A.2) and subjected to cyclical internal air pressure (Table A.1). The structural dynamic response due to impact excitation was measured (Figure A.3) periodically in between loading cycles. The loading was continued until failure.

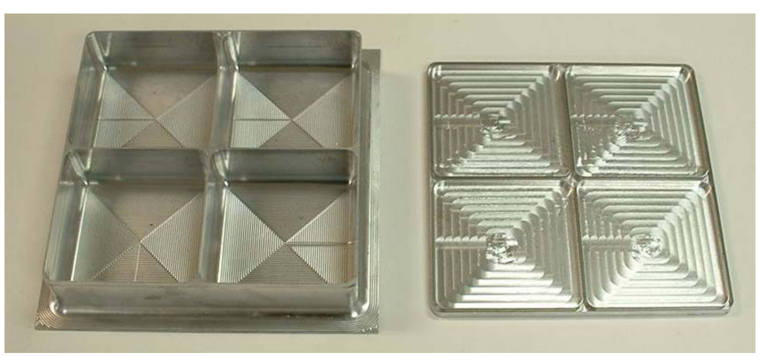

Figure A.1 - GRID-LOCK® test structure

Table A.1 – Loading scheme

Loading stage	Pressure (kPa)	Number of cycles
1	69	40
2	138	40
3	207	40
4	276	40
5	345	40
6	413	40
7	482	40
8	551	40
9	620	40
10	689	40
11	758	40
12	758	40
13	758	80
14	758	80
15	758	100
16	758	100
17	758	100
18	758	150
19	758	150

2.2 Boundary Conditions

The lips in the test structure were clamped with the help of a steel fixture bolted to a table (Figure A.2). This set up for supporting the test component was chosen in order to minimize the influence of boundary conditions in the dynamic response. It may be possible to achieve these test boundary conditions in practice because control surfaces are attached to the airframe on hinges. Therefore they can be removed and tested before being refitted to the aircraft.

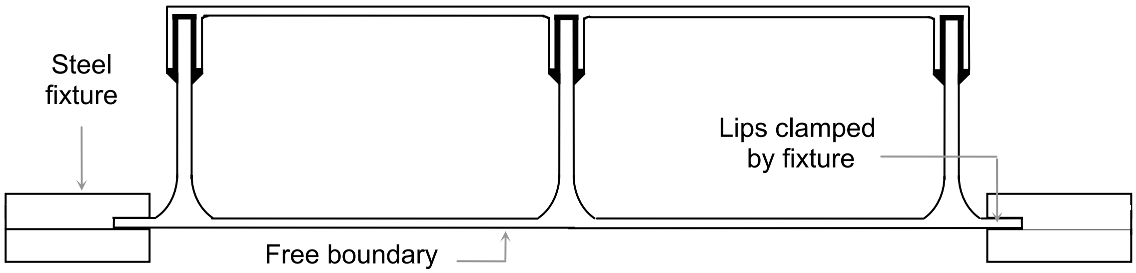

Figure A.2 – Sectional view of the test component
showing applied boundary conditions

2.1 Load Application

The test structure was then internally pressurized (up to 758 kPa) in cycles. The maximum internal pressure level was incremented in stages (Table A.1). Each loading stage was consisted of repeated pressurization to the maximum value and depressurization to atmospheric pressure. This method of load application was adopted to induce fatigue while applying a uniformly distributed load.

2.2 Dynamic Response Measurement

The dynamic response was measured to extract modal parameters. The test structure was excited by means of impact. The impact was imparted at the centre of the test structure with an instrumented impact hammer (PCB 086C03). This location for the impact was chosen because it avoided preferential excitation of only portions of the test structure. The impact amplitudes were kept within the range of 70-80 N in order to avoid any amplitude dependent non-linearity in the response. The response was captured using an accelerometer (PCB 353B65) located as shown in Figure B-3. The response at this location included all modes in the frequency range of interest. The response data was captured for a period of 2 sec at a sampling frequency of 25 kHz using LabVIEW™. The air line was removed during the measurements. The response of the test structure in the unloaded state and the response at the end of each loading stage were recorded.

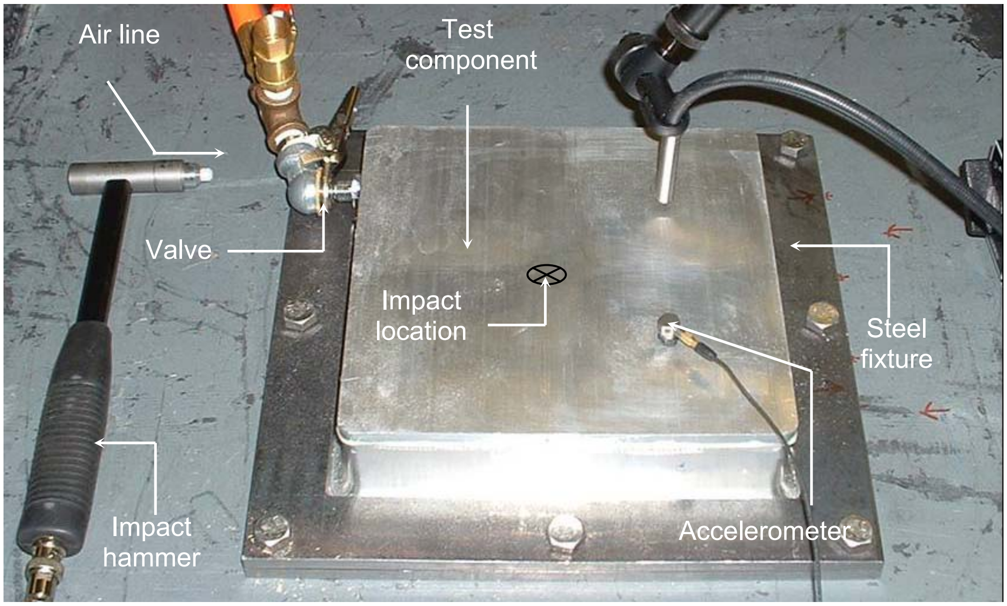

Figure A.3 - Experimental set up

3 Results

The test structure response spectrum (Figure A.4) revealed the presence of closely spaced modes (because of symmetry in the model). Due to the closeness of the modes the response due to a specific mode could not be isolated making it difficult to estimate modal damping ratios. Mode shapes were also not estimated as response measurements at many degrees of freedom would be required. Hence natural frequencies were the only modal parameters extracted from the dynamic response measurements.

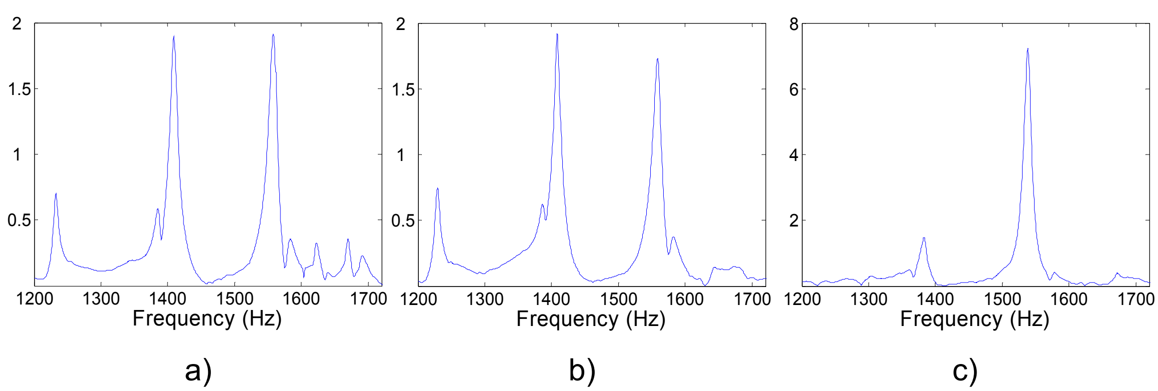

Figure A.4 – Response spectrum a) Before loading, b) Stage 10 and, c) Stage 17

Before commencement of loading, eight vibration modes (1235, 1387, 1411, 1563, 1584 1623, 1674 and 1691 Hz) were identified in the response spectrum (Figure A.4 a). With progression in the loading stages the response spectrum showed distinct changes (Figure A.4). Certain resonant peaks were no longer distinct in the response spectrum during the later loading stages.

Test structure failure occurred after the nineteenth loading stage, evident as a slit in the cover (Figure A.5). This indicated that the fatigue loading had initiated a crack that propagated with further loading resulting in the slit. It must be noted that the tear was visible only after the nineteenth loading stage while the dynamic response shows changes much before.

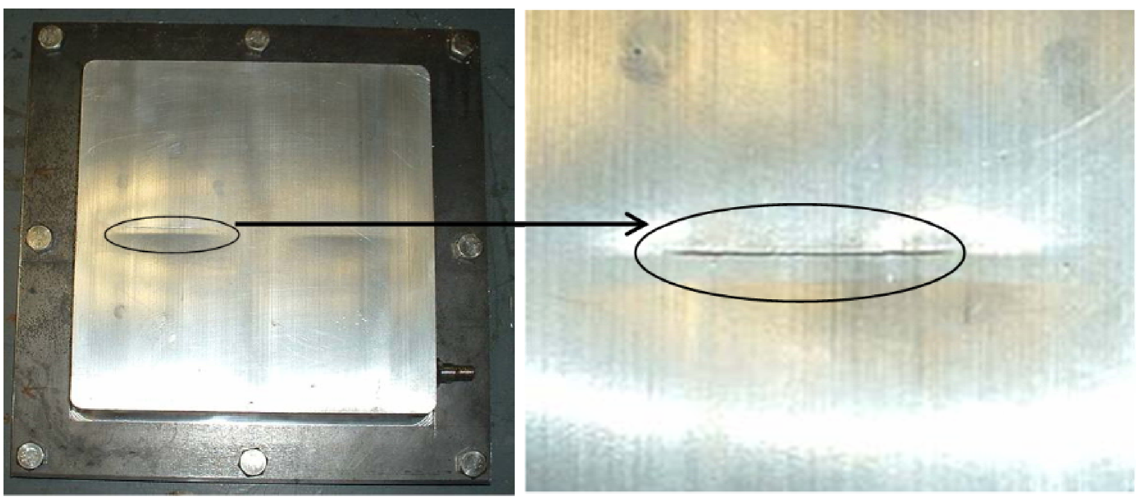

Figure A.5 – Test structure failure

4 Discussion

The significant response changes occurred due to global damage in the test structure. This indicated that vibration testing can be used to determine presence of growth of damage in GRID-LOCK® structures. However, these changes could not be related to specific damage mechanisms (for e.g. the split in Figure A.5). Extracting defect size and location information from natural frequency or frequency response function (FRF) measurements requires the solution to an inverse problem. These problems usually do not have unique solutions (except for structures with simple geometries like beams and plates) because different combinations of defect types, locations, and sizes can produce identical changes in the response.

References

[1] Samuel, P. D. and Pines, D. J. (2005). A Review of Vibration-based Techniques for Helicopter Transmission Diagnostics. *Journal of Sound and Vibration*, *282*(1-2), 475-508.

[2] Trendafilova, . I. (2005). An Investigation on Vibration-based Damage Detection in an Aircraft Wing Scaled Model. *Key Engineering Materials*, *293-294*, 321-328.

[3] Tsyfansky, S. L. and Beresnevich, V. I. (2000). Non-linear Vibration Method for Detection of Fatigue Cracks in Aircraft Wings. *Journal of Sound and Vibration*, *236*(1), 49-60.

[4] Ratcliffe , C. P. (1997). Damage Detection Using a Modified Laplacian Operator on Mode Shape Data. *Journal of Sound and Vibration*, *204*(3), 505-517.

[5] Cornwell, P., Doebling, S. W., and Farrar, C. R. (1999). Application of the Strain Energy Damage Detection Method to Plate like Structures. *Journal of Sound and Vibration*, *224*(2), 359-374.

[6] Kim, J. T. and Stubs, N. (2003). Crack Detection in Beam-type Structures Using Frequency Data. *Journal of Sound and Vibration*, *259*(1), 145-160.

[7] Koh, C. G., See, L. M., and Balendra, T. (1995). Damage Detection of Buildings: Numerical and Experimental Studies. *Journal of Structural Engineering*, *121*(8), 1155-1160.

[8] Worden, K., Manson, G., and Allman, D. (2003). Experimental Validation of a Structural Health Monitoring Methodology: Part I. Novelty Detection on a Laboratory Structure. *Journal of Sound and Vibration*, *259*(2), 323-343.

[9] Worden, K., Manson, G., and Allman, D. (2003). Experimental Validation of a Structural Health Monitoring Methodology. Part II. Novelty Detection on a Gnat Aircraft. *Journal of Sound and Vibration*, *259*(2), 345-363.

[10] Pai, F. P., Kim, B. S., and Chung, J. H. (2004). Dynamics-based Damage Inspection of an Aircraft Wing Panel. *Journal of Intelligent Material Systems and Structures*, *15*(11), 803-821.

[11] Verboven, P., Parloo, E., Guillaume, P., and Van Overmeire, M. (2002). Autonomous Structural Health Monitoring - Part I: Modal Parameter Estimation and Tracking. *Mechanical Systems and Signal Processing*, *16*(4), 637-657.

[12] Worden, K., Manson, G., and Allman, D. J. (2001). An Experimental Appraisal of the Strain Energy Damage Location Method. *Key Engineering Materials*, *204-*, 35-46.

[13] Huth, O., Feltrin, G., and Maeck, J. (2005). Damage Identification Using Modal Data: Experiences on a Prestressed Concrete Bridge. *Journal of Structural Engineering-ASCE*, *131*(12)